7. Penetrative cumulus convection*

7.1 Introduction

The horizontal scale of a cumulus cloud ranges from about 1 to 10 km and this scale is much smaller than the horizontal resolution of the GCM which is about 100～500 km. Therefore, it is impossible to resolve each cumulus cloud in the GCM. On the other hand, the cumulus clouds sometimes extend to about 10 km or more in the vertical direction and play an important role in the vertical transfer of heat, moisture and momentum.

Deep cumuli are a major heating source in the ITCZ and a driving force of Hadley circulation. Thus a cumulus cloud parameterization is essential in simulating global climate by the GCM.

For the parametrization be possible, we have to assume that effects of cumulus cloud ensemble can be determined by the large-scale environment. In other words, the parameterization problem is how to determine grid-scale heat, moistire and momentum changes due to cumulus cloud ensemble in terms of grid-scale fields.

The cumulus parameterization scheme of the MRI• GCM is based on Arakawa-Schubert cumulus parametrization (hereafter abbreviated as the A-S cumulus parameratization. For details, see Arakawa and Schubert, 1974, Lord and Arakawa, 1980, Lord, 1982, Lord, Chao and Arakawa, 1982, etc.). The A-S cumulus parameterization consists of two major parts. One is the cloud model which is described in sections 7.2 and 7.3, and the other is the closure assumption which is described in section 7.4. The discretized form of the parameterization is described in sections 7.5 through 7.8. Section 7.9 describes the parameterization of ice phase cumuli. Appendix 7.1 gives the selected results from the MRI• GCM-I integrations and discussions. Appendix 7.2 gives simple examples of the solution for the mass flux distribution equation.

7.2 Cloud Model I : Modification of the large-scale environment by cumulus clouds

The dry static energy s and the moist static energy h are used in the A-S parameterization. s is an approximately conserved variable during the dry adiabatic process. On the other hand, h is an approximately conserved variable during the moist adiabatic

---

* This chapter is prepared by K. Yamazaki.

process. They are defined by

$$s = c_p T + gz \tag{7.1}$$

$$h = s + Lq = c_p T + gz + Lq \tag{7.2}$$

respectively, where c_p is the specific heat of air under constant pressure, T the temperature, g gravity, z height, L the latent heat per unit mass of water vapor and q the mixing ratio of water vapor.

All the cumulus clouds are assumed to have their roots in the planetary boundary layer (PBL). Other types of clouds are considered separately and described in Chapter 9.

Consider an area which is large enough to contain an ensemble of cumulus clouds but small enough to have a quasi-uniform large-scale environment. There might be various types and stages of cumulus clouds, for example, deep or shallow clouds in developing, mature or decaying stages in the area at a specific moment. Of course, it is impossible to describe each individual cloud by using the GCM. Only the overall statistical effects of the cumulus ensemble can be considered.

We assume that a cloud ensemble can be divided into a cloud subensemble of which thermal stratification in clouds and large-scale effects due to clouds are uniquely defined by a single parameter. We choose the cloud top pressure level P_d as this characteristic parameter instead of the entrainment rate λ as A-S did. λ is the fractional rate of entrainment from environment to the cloud air and assumed to be constant with height. Larger entrainment rate makes the cloud lose its buoyancy sooner, and decrease its cloud height. The highest cloud is realized when the entrainment rate λ is equal to zero. There is a one-to-one correspondence between λ and P_d.

We assume that the height of cloud top is equal to the height of the vanishing buoyancy level. An overshooting effect is neglected. The overshooting, that is, cloud air keeps going upward due to its inertia even after losing its buoyancy, occurs in the real atmosphere. Although overshooting is noticeable for deep cumulonimbus, overshooting depth is small when compared with model's vertical resolution. The detrainment of the cloud air occurs at the level P_d. So, P_d is also called as the detrainment pressure level. Note that P_d is not the height of the individual cloud at the moment. The cloud top does not reach the P_d level until the cloud reaches the mature stage, and the cloud detrains cloud air after it reaches the mature stage. We will discuss the cloud ensemble model in more detail in the next section.

The static energy and moisture budgets for the total area are

$$\rho\frac{\partial\bar{s}}{\partial t}=-\overline{\nabla\cdot(\rho\mathbf{v}s)}-\frac{\partial}{\partial z}(\overline{\rho ws})+L(\sum_i C_i-\varepsilon) \tag{7.3}$$

$$\rho\frac{\partial\bar{q}}{\partial t}=-\overline{\nabla\cdot(\rho\mathbf{v}q)}-\frac{\partial}{\partial z}(\overline{\rho wq})-(\sum_i C_i-\varepsilon) \tag{7.4}$$

where ρ is the density which depends only on z, $\mathbf{v}$ is the horizontal velocity, w the vertical velocity, ∇ the horizontal del operator, C_i the condensation rate of water vapor per unit height in the type-i cloud subensemble, ε the evaporation of the liquid water detrained from the clouds per unit height. The overbar ($\bar{}$) indicates the area average. Storage term in the clouds and radiation effects are neglected.

The total transport of s and q can be expressed by the sum of cloud parts and environmental parts.

$$\overline{\rho ws}=\rho(\sum_i\sigma_i\, w_i\, s_i+(1-\sigma_c)\widetilde{w}\,\widetilde{s})$$

$$=\sum_i M_i\, s_i+\widetilde{M}\,\widetilde{s} \tag{7.5}$$

$$\overline{\rho wq}=\sum_i M_i\, q_i+\widetilde{M}\,\widetilde{q} \tag{7.6}$$

The tilde ($\tilde{}$) indicates the environmental mean value, subscript c indicates total cloud mean value and subscript i indicates the mean value over type-i cloud subensenble. σ_i is the fractional area covered by the type-i cloud subensemble.

$$\sigma_c=\sum_i\sigma_i \tag{7.7}$$

$$\widetilde{M}=\rho(1-\sigma_c)\widetilde{w} \tag{7.8}$$

$$M_c=\rho\sum_i\sigma_i\, w_i \tag{7.9}$$

$$\rho\bar{w}=M_c+\widetilde{M} \tag{7.10}$$

σ_c is the total fractional area covered by all clouds. M_c is the total vertical mass flux by all clouds, $\widetilde{M}$ is the vertical mass flux of environment.

The mass continuity equation is

$$\overline{\nabla\cdot(\rho\mathbf{v})}+\frac{\partial}{\partial z}(\overline{\rho w})=0 \tag{7.11}$$

Neglecting the net lateral horizantal transport across the boundary of the large-scale area by cumulus clouds, the following equations can be obtained

$$\overline{\nabla\cdot(\rho\mathbf{v})}\cong\nabla\cdot(\rho\bar{\mathbf{v}}) \tag{7.12}$$

$$\overline{\nabla\cdot(\rho\mathbf{v}s)}\cong\nabla\cdot(\rho\bar{\mathbf{v}}\bar{s}) \tag{7.13}$$

$$\overline{\nabla\cdot(\rho\mathbf{v}q)}\cong\nabla\cdot(\rho\bar{\mathbf{v}}\bar{q}) \tag{7.14}$$

Then, the continuity equation (7.11) becomes

$$\nabla\cdot(\rho\bar{\mathbf{v}})+\frac{\partial}{\partial z}(\rho\bar{w})=0 \tag{7.15}$$

Using eqs. (7.13) and (7.15), eq. (7.3) can be written as

$$\rho\frac{\partial\bar{s}}{\partial t}=\bar{s}\frac{\partial}{\partial z}(\rho\bar{w})-\rho\bar{\mathbf{v}}\cdot\nabla\bar{s}-\frac{\partial}{\partial z}\sum_i s_i\ M_i$$

$$-\widetilde{s}\frac{\partial\widetilde{M}}{\partial z}-\widetilde{M}\frac{\partial\widetilde{s}}{\partial z}+L(\sum_i C_i-\varepsilon) \tag{7.16}$$

Using eqs. (7.14) and (7.15), eq. (7.4) can be written as

$$\rho\frac{\partial\bar{q}}{\partial t}=\bar{q}\frac{\partial}{\partial z}(\rho\bar{w})-\rho\bar{\mathbf{v}}\cdot\nabla\bar{q}-\frac{\partial}{\partial z}\sum_i q_i\ M_i$$

$$-\widetilde{q}\frac{\partial\widetilde{M}}{\partial z}-\widetilde{M}\frac{\partial\widetilde{q}}{\partial z}-(\sum_i C_i-\varepsilon) \tag{7.17}$$

Assuming no accumulative storage of mass, s and q within the cloud ensemble, we obtain

$$E-D-\frac{\partial M_c}{\partial z}=0 \tag{7.18}$$

$$E\bar{s}-Ds_d-\frac{\partial}{\partial z}(\sum_i M_i\ s_i)-L\sum_i C_i=0 \tag{7.19}$$

$$E\bar{q}-Dq_d-\frac{\partial}{\partial z}(\sum_i M_i\ q_i)-\sum_i C_i=0 \tag{7.20}$$

where subscript d denotes the values in cloud ensemble which detrain at the level under consideration, D is the detrainment and E is the entrainment. We assume that the evaporation of the detrained liquid water takes place at the same level where the water is detrained from the clouds, that is, at the cloud top. Then,

$$\varepsilon=D\ell_d \tag{7.21}$$

where ℓ_d is the mixing ratio of liquid water in the air detrained from the cloud subensemble.

Using eqs. (7.10), (7.18), (7.19), (7.20) and (7.21), eqs. (7.16) and (7.17) can be rewritten as

$$\rho\frac{\partial\bar{s}}{\partial t}=D\ \{(s_d-L\ell_d)-\bar{s}\}+(\bar{s}-\widetilde{s})\frac{\partial\widetilde{M}}{\partial z}$$

$$-\widetilde{M}\frac{\partial \widetilde{s}}{\partial z}-\rho\bar{v}\cdot\nabla\bar{s} \tag{7.22}$$

$$\rho\frac{\partial \bar{q}}{\partial t}=D\ \{(q+\ell)_d-\bar{q}\}+(\bar{q}-\widetilde{q})\frac{\partial \widetilde{M}}{\partial z}$$

$$-\widetilde{M}\frac{\partial \widetilde{q}}{\partial z}-\rho\bar{v}\cdot\nabla\bar{q} \tag{7.23}$$

Note that the cloud condensation term does not appear in eqs. (7.22) and (7.23).

By definition and using (7.7), we obtain

$$\bar{s}=(1-\sigma_c)\widetilde{s}+\sum_i\sigma_i\ s_i=\widetilde{s}+\sum_i(s_i-\widetilde{s})\sigma_i \tag{7.24}$$

$$\bar{q}=(1-\sigma_c)\widetilde{q}+\sum_i\sigma_i\ q_i=\widetilde{q}+\sum_i(q_i-\widetilde{q})\sigma_i \tag{7.25}$$

We assume

$$\sigma_c \ll 1 \tag{7.26}$$

This means that the fractional horizontal area covered by the clouds is much less than unity. We then get

$$\bar{s}\simeq\widetilde{s} \tag{7.27}$$

$$\bar{q}\simeq\widetilde{q} \tag{7.28}$$

In order that eq. (7.28) be a good approximation, the environment must not be extremely dry.

Substituting (7.27) and (7.28) into (7.22) and (7.23) respectively and using (7.10), we finally obtain

$$\rho\frac{\partial \bar{s}}{\partial t}=D\ \{(s-L\ell)_d-\bar{s}\}+M_c\frac{\partial \bar{s}}{\partial z}$$

$$-\rho\bar{v}\cdot\nabla\bar{s}-\rho\bar{w}\frac{\partial \bar{s}}{\partial z}+Q_r \tag{7.29}$$

$$\rho\frac{\partial \bar{q}}{\partial t}=D\ \{(q+\ell)_d-\bar{q}\}+M_c\frac{\partial \bar{q}}{\partial z}$$

$$-\rho\bar{v}\cdot\nabla\bar{q}-\rho\bar{w}\frac{\partial \bar{q}}{\partial z} \tag{7.30}$$

We have restored a radiation term Q_r in eq. (7.29). Except Q_r, the second lines of (7.29) and (7.30) are the large-scale advection terms which can be calculated by large-scale process of the GCM and the first lines of the r. h. s. of (7.29) and (7.30) are the cloud terms which should be given by cumulus parameterization scheme. Adding (7.29) to (7.30), we obtain the time change equation of h,

$$\rho\frac{\partial\bar{h}}{\partial t}=D(h_d-\bar{h})+M_c\frac{\partial\bar{h}}{\partial z}$$

$$-\rho\bar{\mathbf{v}}\cdot\nabla\bar{h}-\rho\bar{w}\frac{\partial\bar{h}}{\partial z}+Q_r \tag{7.31}$$

According to eqs. (7.29) and (7.30), large-scale fields are modified by clouds through two effects. One is the cloud detrainment effect (D-term) which is the first term of the r. h. s. of (7.29) and (7.30), and the other is the term due to compensating downward motion of environmental air (M_c-term) which is the second term of the r. h. s. of eqs. (7.29) and (7.30). Under usual circumstances, D-term acts to cool and moisten the large-scale fields and M_c -term acts in the opposite way.

7.3 Cloud Model II : Cloud ensemble model

M_c (z), the cloud mass flux at level z can be divided into contributions from cloud subensemble as

$$M_c\,(z)=\int_0^{P_b} m(z,\,P_d)\,dP_d \tag{7.32}$$

where P_b is the pressure at the top of the PBL, m(z, P_d) is the cloud mass flux of which the top is P_d (hereafter we call this cloud subensemble as P_d-cloud), at z level. As mentioned in section 7.2, we have adopted P_d as a characteristic parameter instead of an entrainment rate λ. And also λ is assumed to be constant with height for P_d-cloud. Then

$$\frac{\partial}{\partial z}m(z,\,P_d)=\lambda\, m(z,\,P_d) \qquad \text{for } z_b\leqq z<z_d \tag{7.33}$$

where z_b is the PBL top height, z_d the detrainment level (corresponding to P_d). Integrating eq. (7.33), we obtain the subcloud mass flux profile as

$$m(z,\,P_d)=\begin{cases} m_b(P_d)\,e^{\lambda(z-z_b)} & \text{for } z_b\leqq z\leqq z_d \\ 0 & \text{for } z_d<z \end{cases} \tag{7.34}$$

where m_b (P_d) is the mass flux of P_d-cloud at the PBL top. We define normalized cloud mass flux η for convenience.

$$\eta(z)=\begin{cases} e^{\lambda(z-z_b)} & \text{for } z_b\leqq z\leqq z_d \\ 0 & \text{for } z_d<z \end{cases} \tag{7.35}$$

We can write down the budget equation of h and total water content for P_d-cloud in a similar fashion

$$\frac{\partial}{\partial z}\{m(z, P_d)h_c(z, P_d)\}=\lambda \bar{h}(z) \tag{7.36}$$

$$\frac{\partial}{\partial z}\{m(z, P_d)\ [q_c(z, P_d)+\ell(z, P_d)]\}$$

$$=\lambda m(z, P_d)\bar{q}(z)-m(z, P_d)r(z, P_d) \tag{7.37}$$

where h_c (z, P_d), q_c (z, P_d) and ℓ (z, P_d) are h, q and liquid water in the P_d-cloud respectively and $r(z, P_d)$ is the precipitation rate which depends on parameterization of the precipitation process. In the current MRI•GCM, precipitation takes place proportional to the excess water.

Let us consider s, q and h in the clouds. In the clouds, the air is saturated. Neglecting pressure difference between the in-the-cloud and in the environment, we can write

$$q_c(z, P_d)=q_c^*(T_c, P_d)$$

$$\cong\bar{q}^*(z)+\frac{1}{c_p}\left(\frac{\partial\bar{q}^*}{\partial\bar{T}}\right)_p(s_c(z, P_d)-\bar{s}(z)) \tag{7.38}$$

where asterisk (*) denotes the saturation value. Using definition of h and eq. (7.38), we obtain

$$s_c(z, P_d)-\bar{s}(z)\cong\frac{1}{1+\gamma}\ \{h_c(z, P_d)-\bar{h}^*(z)\} \tag{7.39}$$

$$q_c(z, P_d)-\bar{q}^*(z)\cong\frac{\gamma}{1+\gamma}\frac{1}{L}\ \{h_c(z, P_d)-\bar{h}^*(z)\} \tag{7.40}$$

where

$$\gamma\equiv\frac{L}{c_p}\left(\frac{\partial\bar{q}^*}{\partial\bar{T}}\right)_p \tag{7.41}$$

If m_b (P_d) and λ are given, and if h_c and q_c at PBL top, i. e., h_c (z_b, P_d) and q_c (z_b, P_d), are given and further if precipitation parameterization is specified, we can compute h_c (z, P_d), q_c (z, P_d) and ℓ (z, P_d). Since we assume cumulus clouds have their roots within the PBL, it is plausible to assume

$$h_c\ (z_b, P_d)=h_m \tag{7.42}$$

$$q_c\ (z_b, P_d)=q_m \tag{7.43}$$

where h_m and q_m are h and q averaged over the PBL depth.

There then remain two unknowns, i. e., λ and m_b (P_d). To determine λ, non-buoyancy assumption at the cloud top is utilized. The buoyancy is measured by the virtual static energy s_v. s_v is approximately expressed by

$$s_v=s+c_p\ \bar{T}\ (\delta q-\ell) \tag{7.44}$$

where $\delta=0.608$. The non-buoyancy condition is given by $s_v(z_d)=s_{vc}(z_d, P_d)$, *i. e.*,

$$\bar{s}(z_d)+c_p\,\bar{T}(z_d)\,\delta q(z_d)=s_c(z_d,\,P_d)+c_p\,\bar{T}(z_d)\,(\delta q_c(z_d,\,P_d)-\ell\,(z_d,\,P_d)) \tag{7.45}$$

Using (7.39) and (7.40), eq. (7.45) can be rewritten as

$$h_c(z_d,\,P_d)-\hat{h}^*(z_d)=0 \tag{7.46}$$

where

$$\hat{h}^*(z_d)\equiv\bar{h}^*(z_d)-\frac{(1+\gamma)L\varepsilon}{1+\gamma\varepsilon\delta}\,\{\delta\,[\bar{q}^*(z_d)-\bar{q}(z_d)]-\ell\,(z_d,\,P_d)\} \tag{7.47}$$

where $\varepsilon=c_p\,\bar{T}/L$.

Eq. (7.46) is the equation which determines λ from given P_d. Since the equations are too intricate to be solved analytically, an iterative method is adopted in the MRI • GCM-I.

The second term in the r. h. s. of (7.47) is usually small compared with $\bar{h}^*$. Fig. 7.1 shows a typical thermal structure of both clouds and environment in the tropics. As you can see in Fig. 7.1, the highest possible cloud ensemble should have zero entrainment. In that case, h_c is equal to h_m. Then if an inequality $h_m<\bar{h}^*$ (z) holds, there are no clouds that can reach the level z or above that level. In the MRI • GCM-I, the model checks this criterion and if the condition is met, such cloud ensemble is excluded from the possible existing cloud ensemble.

Suppose if we have a situation like the one shown in Fig. 7.2. In the range $\lambda_1<\lambda<\lambda_4$, there are three possible cloud top heights that satisfy the non-buoyancy condition. Branch II

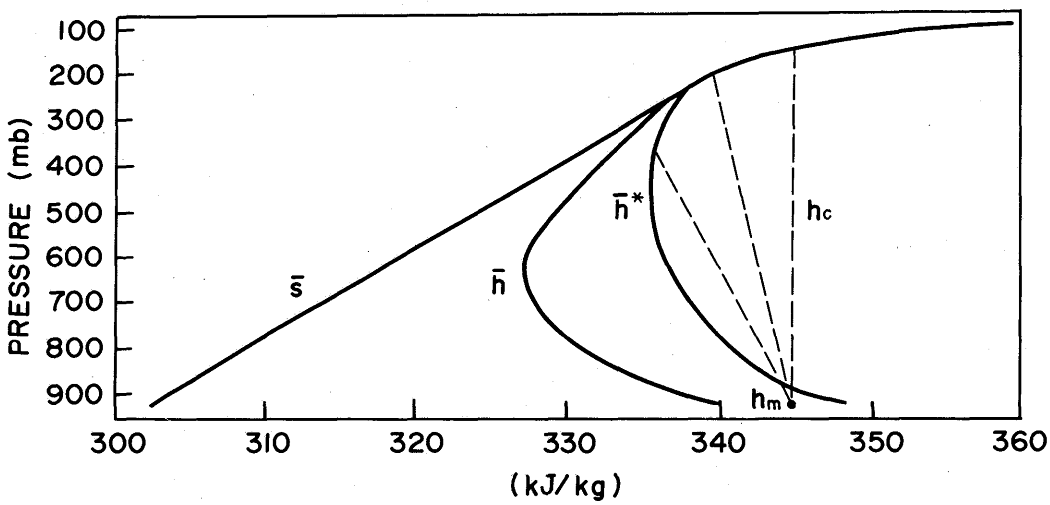

Fig. 7.1 Typical profiles of dry static energy s, moist static energy $\bar{h}$ and saturation moist static energy $\bar{h}^*$. The profiles are taken from Jordan's (1958) mean West Indies sounding. Dashed lines show schematic profiles of moist static energy h in the clouds.

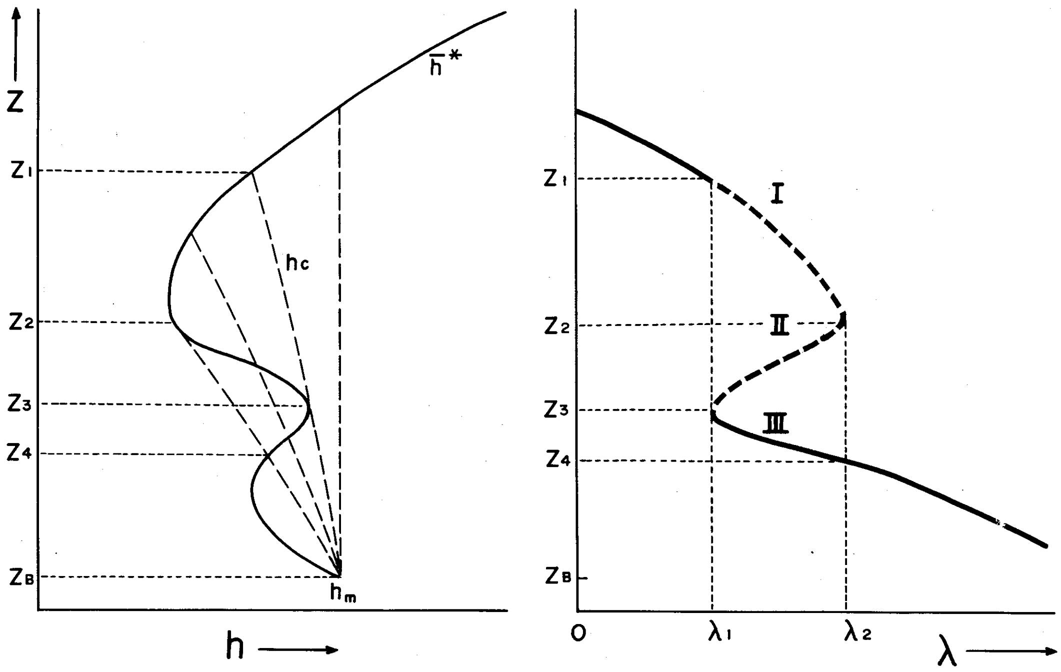

Fig. 7.2 Schematic diagrams of non-buoyancy levels for a special case. In the left panel, the solid line shows saturation moist static energy $\bar{h}^*$ for the environmental air. The dashed lines show the moist energy h in the clouds. The right hand panel shows the variation of the entrainment rate λ with the cloud top height.

in Fig. 7.2 is obviously not realized, because non-buoyancy level is bounded by a positive buoyancy layer above and a negative buoyancy layer below hence the level is unstable. In the real atmosphere, branch I might be possible due to overshooting. However, since we have assumed no-overshooting at the cloud top, branch I should be discarded. Branch III is then the desired choice. The artificial cloud types are excluded currently by checking the λ variation with height.

7.4 The closure assumption : Quasi-equilibrium assumption

As mentioned in the introduction, some kind of statistical balance must exist between the cumulus cloud ensemble and the large-scale (grid-scale) fields for a cumulus parametrization. When the large-scale processes tend to generate the moist convective instability, the cumulus cloud ensemble tends to destruct the instability mainly by compensating subsidence in the environment. In the A-S parameterization, this balance is stated by the quasi-equilibrium of "cloud work function". The cloud work function A (P_d) is defined as a work done by the buoyancy force per unit cloud-base mass flux, i. e.,

$$A(P_d)=\int_{z_b}^{z_d}\frac{g}{\bar{T}(z)}\eta(z,\ P_d)\ [T_{vc}(z,\ P_d)-\bar{T}_v(z)]\ dz \tag{7.48}$$

where $T_{vc}(z,\ P_d)$ and $\bar{T}_v(z)$ are the subensemble and environmental virtual temperature respectively. Note that the cloud work function depends upon the thermal stratification only. Using moist static energy, eq. (7.48) can be written as

$$A(P_d)=\int_{z_b}^{z_d}\frac{g\ [1+\gamma(z)\,\varepsilon(z)\,\delta]}{c_p\bar{T}(z)\ [1+\gamma(z)]}\eta(z,\ P_d)\ [h_c(z,\ P_d)-\hat{h}^*(z)]\ dz \tag{7.49}$$

The work $A(P_d)$ generates the kinetic energy of cloud subensemble, while the cloud-scale dissipation acts to prevent the increase of the cloud kinetic energy. Thus, the kinetic energy budget for the cloud subensemble is described as

$$\frac{d}{dt}K(P_d)dP_d=\ [A(P_d)-D(P_d)]\ m_b(P_d)dP_d \tag{7.50}$$

where $K(P_d)\ dP_d$ is the cloud-scale kinetic energy for the subensemble P_d with cloud top between P_d and P_d+dP_d, $D\ (P_d)$ is the cloud-scale kinetic energy dissipation per unit cloud -base mass flux. For the first approximation, $D\ (P_d)$ depends upon only cloud depth. When we consider the time scale much longer than the decay time of clouds, the l. h. s. of (7.50) can be neglected. Eq. (7.50) then becomes

$$A(P_d)\approx D(P_d) \qquad \text{for} \quad m_b(P_d)>0 \tag{7.51}$$

In case that $A\ (P_d)$ is less than $D\ (P_d)$, the cloud can not be sustained. Therfore,

$$m_b(P_d)=0 \qquad \text{for } A(P_d)<D(P_d) \tag{7.52}$$

These equations (7.51) and (7.52) express the "kinetic energy quasi-equilibrium" for each cumulus subenemble. Equation (7.51) poses very strict constraint for the stratification, because $A\ (P_d)$ is the function of the stratification and cloud depth, while $D\ (P_d)$ is the function of cloud depth only. When cloud subensemble exists ($m_b\ (P_d)>0$), the temperature and/or humidity must change with time, but $A\ (P_d)$ must remain constant. This implies temperature field and moisture field can not vary independently. When clouds exist the stratification remains "neutral" in a sence.

Let it be clear by taking the derivative of eq. (7.51) with respect to time

$$\frac{d}{dt}A\ (P_d)\approx\frac{d}{dt}D\ (P_d)\approx 0 \tag{7.53}$$

The time derivative of $A\ (P_d)$ can be divided into two parts, one representing the effects of cumulus feedback on the large-scale fields and the other representing the effects of the large

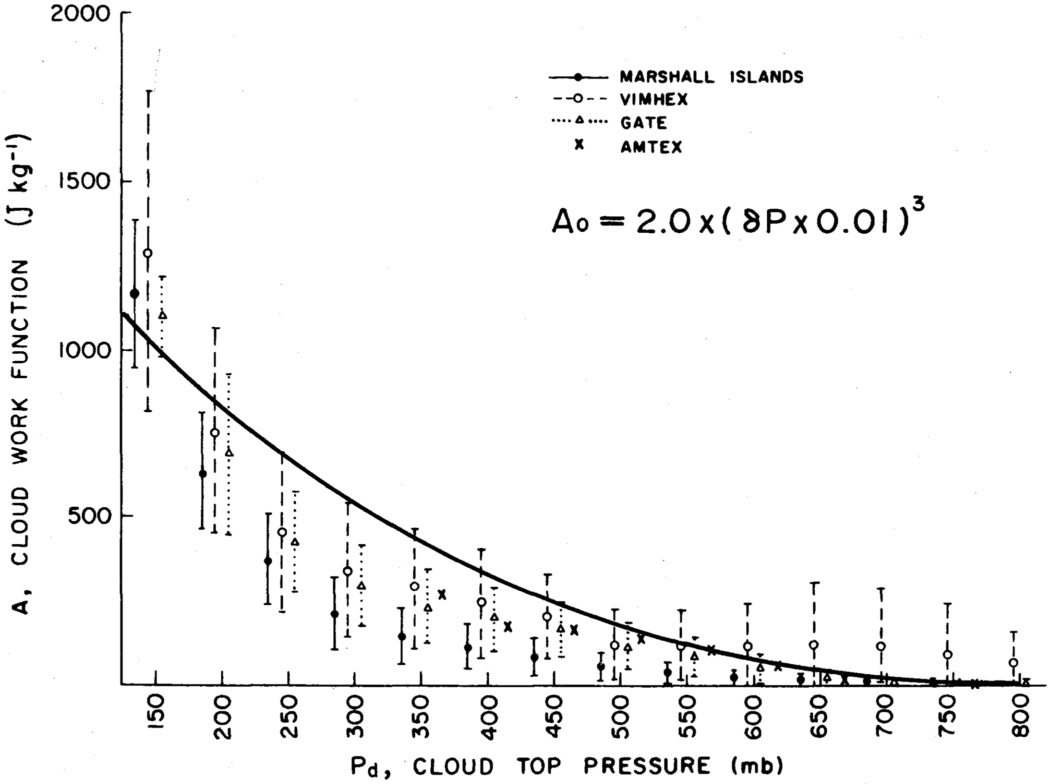

Fig. 7.3 Mean values and standard deviations of the cloud work function versus cloud top pressure P_d calculated from the Marshall Islands, VIMHEX, GATE and AMTEX datasets. Error bars represent one standard deviation from the mean. Adopted from Fig. 9 of Lord and Arakawa (1980). Thick solid line is added to show the base line cloud work function A_0 (P_d) used in the MRI • GCM-I.

-scale process. Eq. (7.53) then becomes

$$\left[\frac{d}{dt}A(P_d)\right]_{CU}+\left[\frac{d}{dt}A(P_d)\right]_{LS}=\frac{d}{dt}A(P_d)$$

$$\cong 0 \tag{7.54}$$

where the subscript CU refers to cumulus effects and LS refers to the large-scale effects.

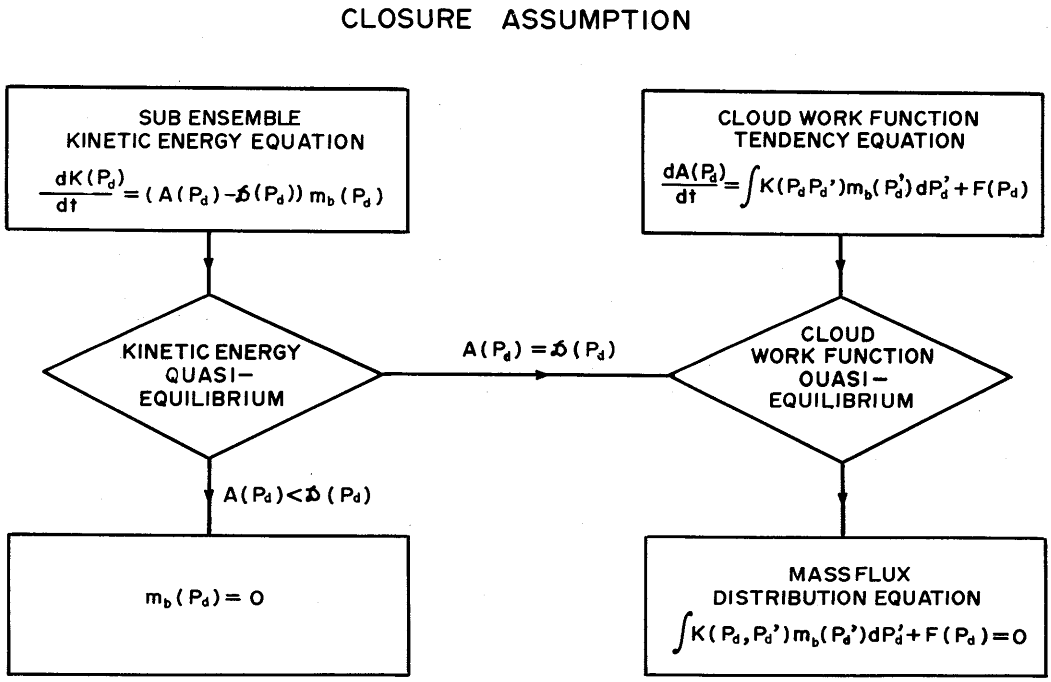

Fig. 7.4 A summary of the derivation of the mass flux distribution equation using the kinetic energy quasi-equilibrium and the cloud work function quasi-equilibrium. Adopted from Fig. 2 of Lord and Arakawa (1980) with minor changes.

The large-scale term is called the large-scale forcing and denoted as F (P_d). Positive F (P_d) means destabilization for the cloud subensemble. The cumulus term represents the cloud -cloud interaction and can be written as

$$\left[\frac{d}{dt}A\ (P_d)\right]_{ct} = \int_0^{Pb} K\ (P_d,\ p')\ m_b\ (p')\ dp' \tag{7.55}$$

where the kernel K (P_d, p') represents the effect of p' cloud on P_d cloud. Since cumulus clouds tend to stabilize the stratification, typically the kernel K (p, p') takes negative value. From eqs. (7.54) and (7.55), we obtain

$$\int_0^{Pb} K\ (P_d,\ p')\ m_b\ (p')\ dp' + F\ (P_d) = 0 \qquad \text{for } m_b\ (P_d) > 0 \tag{7.56a}$$

This is a statement of "cloud-work function quasi-equilibrium" for cumulus ensemble. In case of zero m_b (P_d), cloud work function may be reducing with time.

$$\int_0^{Pb} K\ (P_d,\ p')\ m_b\ (p')\ dp' + F\ (P_d) \leqq 0 \qquad \text{for } m_b\ (P_d) = 0 \tag{7.56b}$$

D (P_d) is an intrinsic cloud subensemble variable and does not depend on the large-scale fields. From eq. (7.51), $D(P_d)$ can be estimated by computing the observed cloud work function. Lord and Arakawa (1980) computed the cloud work function for various geographical areas and situations (Fig. 7.3). The thick solid line in Fig. 7.3 is the characteristic cloud work function A_0 (P_d) currently used in the MRI•GCM-I (see section 7.6.2 for details).

The closure assumption of the A-S cumulus paramerization is summarized in Fig. 7.4.

7.5 The vertical structure of the discrete model and the discretized form of the cloud model.

This section describes the discretized form of the parametrization whose continuous form is described in sections 7.2 and 7.3. In the MRI•GCM-I preadjustments of the large-scale thermodynamic structure are made before the cumulus parameterization is applied. The preadjustments include dry convective adjustment, middle level convection and large-scale precipitation, and are performed in this order. Details of the preadjustments are found in Chapter 9.

7.5.1 The vertical structure of the discrete model

The vertical structure of the MRI • GCM-I is shown in Fig. 7.5. The left hand side of the figure shows the vertical structure of the large-scale model. The dashed lines indicate levels with integer index k where the large-scale temperature T (k) and water vapor mixing ratio q (k) are predicted. In other chapters the levels are identified as "odd levels". The solid lines indicate half-integer levels where the large-scale vertical p-velocity is defined ("even levels"). The region bounded by levels $k-1/2$ and $k+1/2$ is referred to as "layer k". The PBL top in the MRI • GCM-I is not the sigma surface. Although the top of the PBL is assumed within the lowest layer LM in this figure, it can be in upper layers, of course. Thermal structures within the PBL are determined in a way described in Chapter 8.

The right hand side of Fig. 7.5 shows the vertical indices for the cumulus parameterization. The part of layer LM above the PBL is referred to as layer KB (In other chapters, this layer is identified as E layer. See Fig. 8.4 for example.). When the PBL top lies within the lowest layer, LM is equal to KB.

The cloud top is placed at the integer levels as shown in Fig. 7.6. In the following it is convenient to identify each cloud ensemble with the vertical index of each cloud top. The left-hand ensemble in Fig. 7.6 is the type-i cloud, for example. Height-dependent variables of a cloud subensemble are represented by double arguments. The subensemble vertical mass flux for type-i cloud, defined at the half-integer level, is denoted by m (i, $k-1/2$) and can be

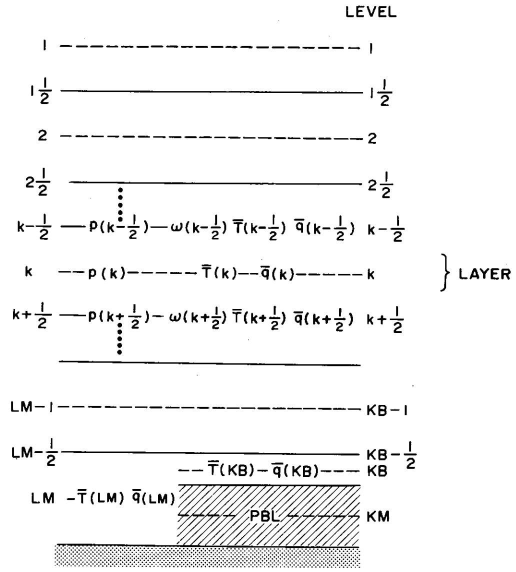

Fig. 7.5 The vertical structure and indices of the model. Indices on the r. h. s. are used in the cumulus parameterization model. Ones on the 1. h. s. are for the large-scale model. KM is the index of the PBL and KB denotes the part of the layer immediately above the PBL.

expressed as

$$m\,(i,\ k-1/2)=\eta(i,\ k-1/2)\ m_b\,(i) \tag{7.57}$$

where m_b (i) is the cloud-base mass flux for type-i cloud and η (i, k−1/2) is the normalized subensemble vertical mass flux at level k−1/2. In general, the first argument corresponds to the cloud type and the second one corresponds to the layer concerned. The entrainment of environment of environment air, denoted by E (i, k), occurs at all integer levels penetrated by the cloud including the cloud top layer. The detrainment of cloud air, denoted by D (i), occurs only at the cloud top level (see Fig. 7.6).

7.5.2 The mass budget

A discretized form of the subensemble mass budget equation (7.33) of section 7.3 for layer k, $k \neq i$, can be written as

$$\frac{\eta(i,\ k-1/2)-\eta(i,\ k+1/2)}{\Delta z(k)}=\lambda\,(i)\,\eta(i,\ k+1/2) \tag{7.58}$$

from which

$$\eta(i,\ k-1/2)=\eta(i,\ k+1/2)\ \left[1+\lambda\,(i)\,\Delta z(k)\right] \tag{7.59}$$

is obtained. HereΔz (k)=z (k−1/2)−z (k+1/2). The mass budget for the cloud top layer

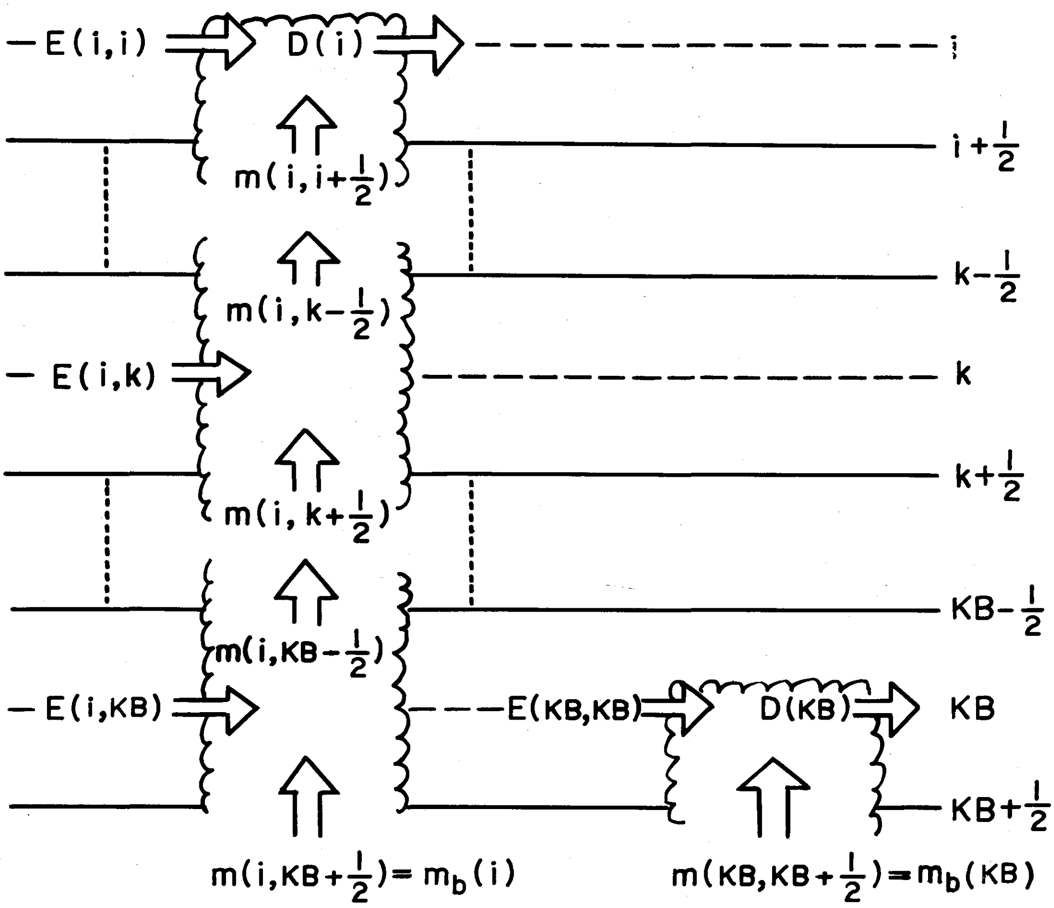

Fig. 7.6 Vertical structures of type-i cloud (on the left) and type-KB cloud (on the right). Entrainment E takes place at all integer levels penetrated by the cloud including the cloud top level, while detrainment D takes place at the cloud top level only. The subensemble cloud mass flux is calculated at the half-integer levels.

$k=i$ is given by

$$d(i)=\eta(i,\ i+1/2)\ [1+\lambda(i)\Delta\hat{z}(i)] \tag{7.60}$$

where d(i) is the cloud top mass detrainment integrated over layer i and normalized by the cloud-base mass flux $m_b(i)$, and $\Delta\hat{z}\ (i)=z\ (i)-z\ (i,\ 1/2)$.

7.5.3 The moist static energy budget

For layer k and type-i cloud, let h(i, $k+1/2$) be the subensemble moist static energy before entrainment and let h(i, $k-1/2$) be the subensemble moist static energy after

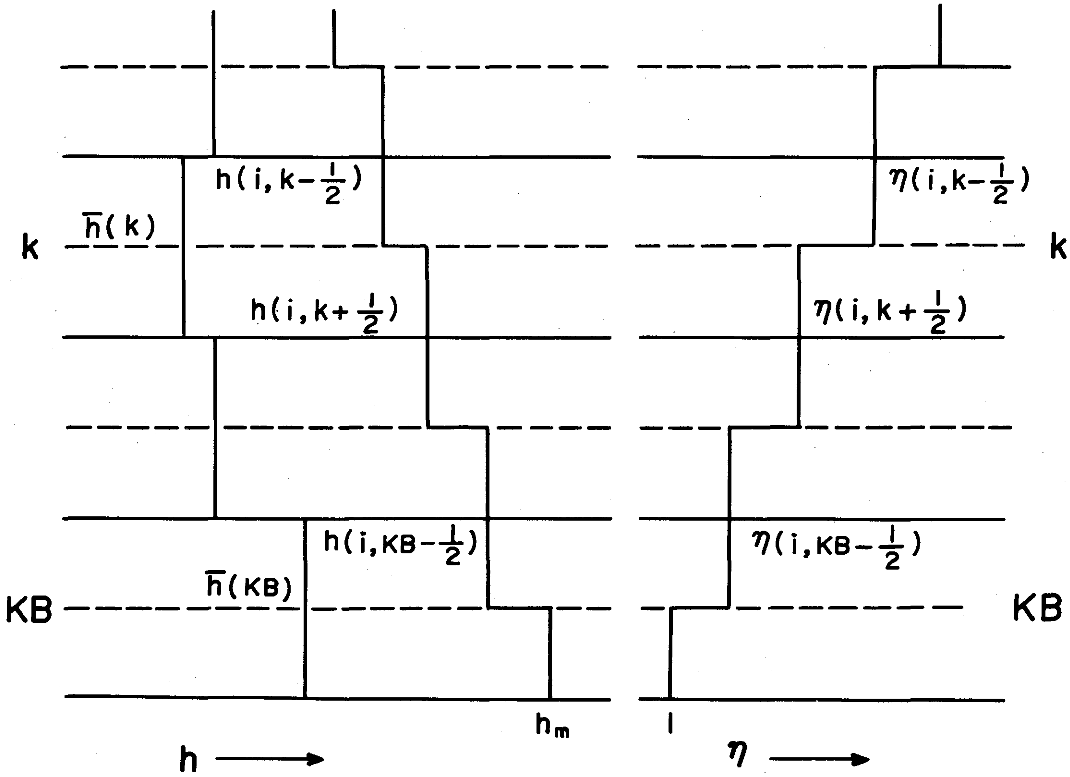

Fig. 7.7 Typical vertical profiles of normalized cloud mass flux η and moist static energy h for the type-i cloud. The 1. h. s. profile shows h for the environment.

entrainment (Fig. 7.7). Then the discretized subensemble moist static energy budget integrated over layer k can be written as

$$\eta\ (i,\ k-1/2)\ h\ (i,\ k-1/2)=\eta\ (i,\ k+1/2)\ h\ (i,\ k+1/2) + \lambda(i)\Delta z\ (k)\ \eta\ (i,\ k+1/2)\ \bar{h}\ (k) \qquad (7.61)$$

From eq. (7.61), we obtain

$$h\ (i,\ k-1/2)=\frac{h\ (i,\ k+1/2)+\lambda(i)\Delta z\ (k)\ \bar{h}\ (k)}{1+\lambda(i)\Delta z\ (k)} \qquad (7.62)$$

When k=KB in eqs. (7.62), h (i, KB+1/2)=h_m, the mean h in the PBL (see (8.36)). In the cloud -top detrainment layer (7.62) becomes

$$\hat{h}\ (i)=\frac{h\ (i,\ i+1/2)+\lambda\ (i)\Delta z\ (i)\ \bar{h}\ (i+1/4)}{1+\lambda\ (i)\Delta\hat{z}\ (i)} \qquad (7.63)$$

where $\hat{h}$ (i) is the moist static energy at the cloud-top and $\bar{h}$ (i+1/4)=0.5 • ($\bar{h}$ (i)+$\bar{h}$ (i+1/2)). Sequential substitutions of (7.62) into (7.63) with i+1≦k≦KB result in a complicated expression for $\hat{h}$ (i) which depends on the known h_m, h (k) for $i \leqq k \leqq KB$ and the unkown λ (i). By requiring non-buoyancy at the cloud-top, i. e., $\hat{h}(i) = \hat{h}^*(i)$ (see eq. (7.46) and (7.47)), λ (i) may be determined iteratively as shown in the section 7.5.5.

7.5.4 The total water budget

The budget for total cloud water is calculated in two steps as described below. Let q^t (i, k+1/2) be the value of the total cloud water (vapor and suspended liquid water) mixing ratio entering layer k from below for type-i cloud. And let q(i, k) be the value after entrainment but before the precipitation process. And let q^t (i, k−1/2) be the value after the precipitation process, which also is the value leaving layer k. Also, let $q_l(i,k)$ be the cloud suspended liquid water mixing ratio before precipitation, and q_l^t (i, k−1/2) the value after the precipitation process.

The first step in the total cloud water budget is calculated in the similar manner as eq. (7.62)

$$q\ (i,\ k) = \frac{q^t\ (i,\ k+1/2) + \lambda\ (i)\Delta z\ (k)\ \bar{q}\ (k)}{1+\lambda\ (i)\Delta z\ (k)} \tag{7.64}$$

where $\bar{q}$ (k) is the large-scale total water mixing ratio. Since the large-scale precipitation process is implemented before the cumulus parameterization is applied, $\bar{q}$ (k) is identical to water vapor mixing ratio $\bar{q}_v$ (k). When k=KM in eq. (7.64), q (i, KB+1/2)=q_m.

The second step in the total water budget calculation determines the amount of precipitation produced in layer k from type-i cloud. When the cloud is saturated at level k the cloud water vapor mixing ratio q_v (i, k) is calculated from a discretized form of eq. (7.40) of section 7.3,

$$q_v\ (i,\ k) = \bar{q}_v^*\ (k) + \frac{\gamma\ (k)}{[1+\gamma\ (k)]\ L}\ [h\ (i,\ k-1/2) - \bar{h}^*\ (k)] \tag{7.65}$$

where $\gamma\ (k) = L/c_p\ [\partial \bar{q}_v^*\ (k)/\partial T]_p$.

The resulting suspended liquid water mixing ratio before precipitation is

$$q_\ell (i,\ k) = q\ (i,\ k) - q_v\ (i,\ k) \tag{7.66}$$

Part of q_ℓ(i, k) is converted into precipitation by assuming a constant conversion rate per unit height. Therefore

$$q_\ell^t\ (i,\ k-1/2) = q_\ell (i,\ k) - C_0 \Delta z\ (k)\ q_\ell^t\ (i,\ k-1/2) \tag{7.67}$$

from which

$$q_{\ell}^{t}\ (i,\ k-1/2)=\frac{q_{\ell}(i,\ k)}{1+C_0\Delta z\ (k)} \tag{7.68}$$

A conversion coefficient C_0 in eqs. (7.67) and (7.68) is set to 0.004 m^{-1} for the cloud-top layer and 0.002 m^{-1} for the rest of layers. Lord (1978) has shown that this values of C_0 produce good agreement with observed liquid water content in hurricanes summarized by Ackerman (1963). Similar calculation by Schubert (1973) for Marshall Islands data also have shown good agreement with observations.

7.5.5 The solution procedure for λ(i)

Let a functional F $[\lambda(i)]$ be defined by

$$F\ [\lambda(i)]=(\hat{h}\ (i)-\hat{h}^*\ (i))\ \eta\ (i,\ i) \tag{7.69}$$

where F depends on λ(i) through $\hat{h}$(i), η(i, i) and $\hat{h}^*$(i) (see eq. (7.47)). If the virtual temperature effects are neglected, $\hat{h}^*$ (i) does not depend on λ (i). Since virtual temperature effects are small, dependence of $\hat{h}^*$ (i) on λ (i) is weak. The non-bouyancy condition at cloud top is

$$F\ [\lambda(i)]=0 \tag{7.70}$$

which is an implicit equation for λ(i) and may be solved iteratively by the Newton-Raphson method. Let ν be the number of iterations and let λ_ν (i) be λ(i) at the ν-th iteration. For the first guess, $\lambda_1(i)=0$ is used. For succeeding iterations, $\lambda_{\nu+1}(i)$ can be obtained as

$$\lambda_{\nu+1}(i)=\lambda_\nu(i)-\frac{F\ [\lambda_\nu(i)]}{F'\ [\lambda_\nu(i)]} \tag{7.71}$$

where $F'[\lambda_\nu(i)]$ is the value of the first derivative of $F[\lambda(i)]$ with respect to λ(i) at $\lambda(i)=\lambda_\nu(i)$. When $F'[\lambda_\nu(i)]$ is computed, $\hat{h}^*$(i) is assumed to be constant with respect to λ. The iteration is repeated until $|\ \hat{h}(i)-\hat{h}^*(i)\ | \leqq 1.0$ J kg^{-1} which is equivalent to a cloud-top/environment temperature difference of about 10^{-3} K.

In case that the iteration does not converge after 15 iterations for type-i cloud, such cloud is discarded. Also if cloud air is not saturated at the cloud top, such cloud type is discarded. After we get all possible cloud types, the order of computed values of λ is checked according to the consideration mentioned in section 7.3.

7.6 The discrete form of the mass flux distribution equation

7.6.1 The discretized equation

The mass flux distribution equation for the continuous case is given by (7.46) in section 7.4. This equation is discretized and integrated over a time step Δt_d (see Fig. 5.1) and is written as

$$m_b\ (i)\Delta t_d > 0 \qquad \text{and}$$

$$\sum_{j=1}^{i\,max} [K\ (i,\ j)\ m_b(j)\Delta t_d] + F\ (i)\Delta t_d = 0 \tag{7.72a}$$

or

$$m_b\ (i)\Delta t_d = 0 \qquad \text{and}$$

$$\sum_{j=1}^{i\,max} [K\ (i,\ j)\ m_b(j)\Delta t_d] + F\ (i)\Delta t_d \leqq 0 \tag{7.72b}$$

for $1 \leqq i \leqq i_{max}$. Here i_{max} is the number of possible existing subensembles ; K (i, j), for $1 \leqq i,\ j \leqq i_{max}$, is a discrete form of the mass flux kernel which gives the stabilization of the type-i cloud subensemble through modification of the large-scale environment by the type-j cloud subensemble ; and F (i) is the large-scale forcing for the type-i cloud subensemble. Note that there is an equal sign in the second equation of (7.72b). This equal sign is placed in order to assure the existence of solution (there is no equal sign in Arakawa and Schubert's eq. (74) *etc.*). Let us consider the simplest case in which $i_{max} = 1$. Then equation becomes

$$\begin{cases} m_b\Delta t_d > 0 \qquad \text{and} \\ K\ m_b\Delta t_d + F\Delta t_d = 0 \end{cases} \tag*{(7.72a)$'$}$$

or

$$\begin{cases} m_b\Delta t_d = 0 \qquad \text{and} \\ K\ m_b\Delta t_d + F\Delta t_d \leqq 0 \end{cases} \tag*{(7.72b)$'$}$$

where we omitted suffices for simplicity. If an equal sign in the second equation of (7.72b)′ is dropped, (7.72b)′ becomes

$$\begin{cases} m_b\Delta t_d = 0 \qquad \text{and} \\ K\ m_b\Delta t_d + F\Delta t_d < 0 \end{cases} \tag*{(7.72c)$'$}$$

If F is exactly zero and $K \neq 0$, $m_b = 0$ is the solution of the equations of (7.72a)′ and (7.72b)′. However there are no solutions for equations (7.72a)′ and (7.72c)′. This modification is also justified from the physical consideration. Under completely neutral and steady condition, the cloud work function also must be steady and m_b should be zero.

7.6.2 The large-scale forcing

The large-scale forcing for the type-i cloud subensemble is defined in section 7.4 as the change in cloud work function due to large-scale processes. Let the large-scale thermodynamical variables (temperature, water vapor mixing ratio, *etc.*) be denoted collectively by $\bar{\psi}_0$ where the subscript denotes a particular time t_0. The effects of the large-scale processes (*e.g.*, large-scale vertical and horizontal advections of temperature and moisture, radiative heating and boundary layer processes) are added over Δt_d to give the change

$$\bar{\psi}' = \bar{\psi}_0 + \left[\frac{\partial \bar{\psi}}{\partial t}\right]_{LS} \Delta t_d \tag{7.73}$$

where $[\partial \bar{\psi}/\partial t]_{LS}$ represents the time change of $\bar{\psi}$ due to the large-scale processes. Let the cloud work function for the type-i cloud subensemble calculated from $\bar{\psi}'$ be denoted by A′(i). The large-scale forcing is then written as

$$F\ (i) = \frac{A'(i) - A_0(i)}{\Delta t_d} \tag{7.74}$$

Although $A_0(i)$ is the cloud work function at t_0 by definition, $A_0(i)$ can be replaced by a characteristic value for the type-i cloud subensemble. The replacement of $A_0(i)$ by a characteristic value is justified by the kinetic energy quasi-equilibrium (*e. g.*, see (7.51) and the following discussion). Lord and Arakawa (1880) showed that when both large-scale and cloud processes are operating, cloud work function values fall into a well-defined narrow range for each subensemble, and the variation in the cloud work function becomes negligible over the time scale of the large-scale motions. It follows that the values based on observed time-mean cloud work function may be used as A_0 (i) in the GCM. Modification of $\bar{\psi}'$ by the cumulus mass flux obtained from (7.74) should restore A′(i) to the characteristic value $A_0(i)$. Currently,

$$A_0(i) = 2 \times 10^{-6}\ \{P_b - p\ (i)\}^3 \tag{7.75}$$

is used for simplicity, where P_b and p (i) are values in mb (see Fig. 7.3).

7.6.3 The mass flux kernel

The kernel element K(i, j) is defined as the time rate of change of the cloud work function for the type-i cloud subensemble due to modification of the large-scale environment by a unit mass flux of the type-j cloud subensemble. The changes in the large-scale environment by the cumulus terms are given by the first lines of the r. h. s. of (7.29) and (7.30). These terms are written in the discrete form as eqs. (7.82) and (7.83) in section 7.8. After the above definition of K(i, j), it is evaluated in the following way. The large-scale environment, represented by $\bar{\psi}'$ from eq. (7.73) is modified by an arbitrarily chosen amount of mass per unit area from the type-j cloud subensemble m_b'' (j)$\Delta t''$ to give

$$\bar{\psi}''(k)=\bar{\psi}'(k)+\delta_j\,[\bar{\psi}(k)]\;m_b''\;(j)\Delta t'' \qquad (7.76)$$

Here the index k has been added to indicate the level in the large-scale model, $\delta_j\,[\bar{\psi}(k)]$ refers to the time rate of change in $\bar{\psi}(k)$ per unit mass flux of the type-j cloud subensemble, and the double prime denotes a value used in the mass flux kernel element calculation. A new fractional entrainment rate $\lambda''(i)$ and the cloud work function $A''(i)$ are then calculated for the type-i cloud subensemble using λ''. Finally, the kernel element is calculated as

$$K\,(i,\,j)=\frac{A''(i)-A'(i)}{m_b''(j)\Delta t''} \qquad (7.77)$$

The test mass flux $m_b''\;(j)\Delta t''$ is arbitrarily chosen to be 100 kg m^{-2}. The choice of a particular value for $m_b''\;(j)\Delta t''$ is not important because non-linearity of $A''(i)-A'(i)$ on the test mass flux is weak.

Since a given cloud type tends to stabilize the large-scale fields for all cloud types, the kernel elements K (i, j) should be typically negative. In particular, a given subensemble must reduce its own cloud work function, *i. e.*, for all i,

$$K\,(i,\,i)<0 \qquad (7.78)$$

Otherwise, such cloud subensemble is unstable and develops by itself. However, under very unusual circumstances, the calculated value of K (i, i) may not satisfy (7.78) primarily due to too coarse a vertical resolution. Therefore, K (i, i) $=-\xi$, where ξ is arbitrarily chosen to be

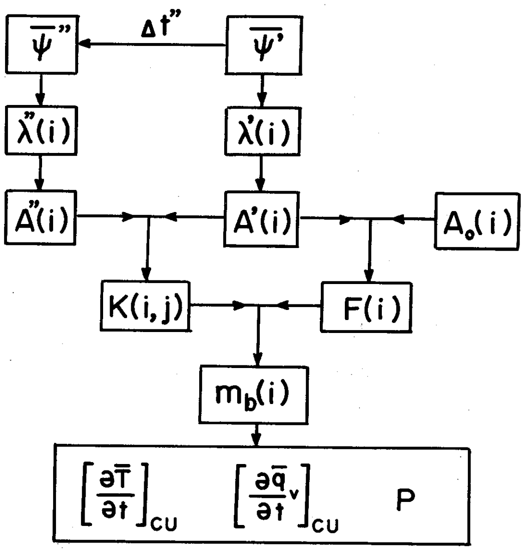

Fig. 7.8 A schematic diagram of the procedure applying the discretized cumulus model to a large-scale prognostic model. Adopted from Fig. 5 of Lord *et al.* (1982).

5×10^{-3} J m^{-2} kg, is enforced. Note that when $i=i_{max}=1$, eq. (7.78) is a necessary and sufficient condition for the existence of a unique solution of $m_b\Delta t_d$ for (7.72a)′ and (7.72b)′. Incidentally, the mass flux distribution equations (7.72a) and (7.72b) do not necessarily have their unique solution. This mathematical aspect of equations is discussed in Appendix 7.2.

The procedure for obtaining the cloud base mass flux distribution in the GCM is summarized in Fig. 7.8. The thermodynamical variables after modification by the large-scale processes ($\bar{\psi}'$) are the inputs to this cumulus parameterization scheme. From these variables $\lambda'(i)$ and $A'(i)$ are calculated for each subensemble. Using an empirically defined characteristic cloud work function $A_0(i)$, the large-scale forcing is calculated from eq. (7.74). The large-scale environment is then modified by the test mass flux $m_b''(j)\Delta t''$ to produce thermodynamical variables $\bar{\psi}''$ which are then utilized to calculate a new value of the cloud work function $A''(i)$. The kernel elements are calculated from (7.77) and the $m_b(i)$ are determined from the mass flux distribution equations (7.72a) and (7.72b). The method to solve the equations (7.72a) and (7.72b) is described in the next section.

7.6.4 The cloud work function

To compute the large-scale forcing and the kernel elements, the cloud work function must be computed. The discrete form of the cloud work function is written straightforwardly from eq. (7.49) as

$$A(i)=\sum_{k'=i+1}^{KB+1}\frac{g}{c_pT(k'-1/2)}\eta(i,k'-1/2)\times\left[\frac{h(i,k'-1/2)-\hat{h}^*(i,k'-1/2)}{1+\gamma(k'-1/2)}\right]\left[z(k'-1)-z(k')\right] \tag{7.79}$$

where $z(KB+1)=z_b$.

7.7 Solution of the mass flux distribution equation

The mass flux distribution eqaution (7.72) must be solved subject to the constraints of non-negative $m_b(i)$ and the inequality conditions (7.72b). For convenience, eq.(7.72) is rewritten here, replacing $m_b(i)\Delta t_d$ with $x(i)$ and $F(i)\Delta t_d$ with $c(i)$.

$$\begin{cases} x(i)>0 \qquad \text{and} \\ \sum_{j=1}^{i\,max} K(i,j)\,x(j)+c(i)=0 \end{cases} \tag{7.80a}$$

or

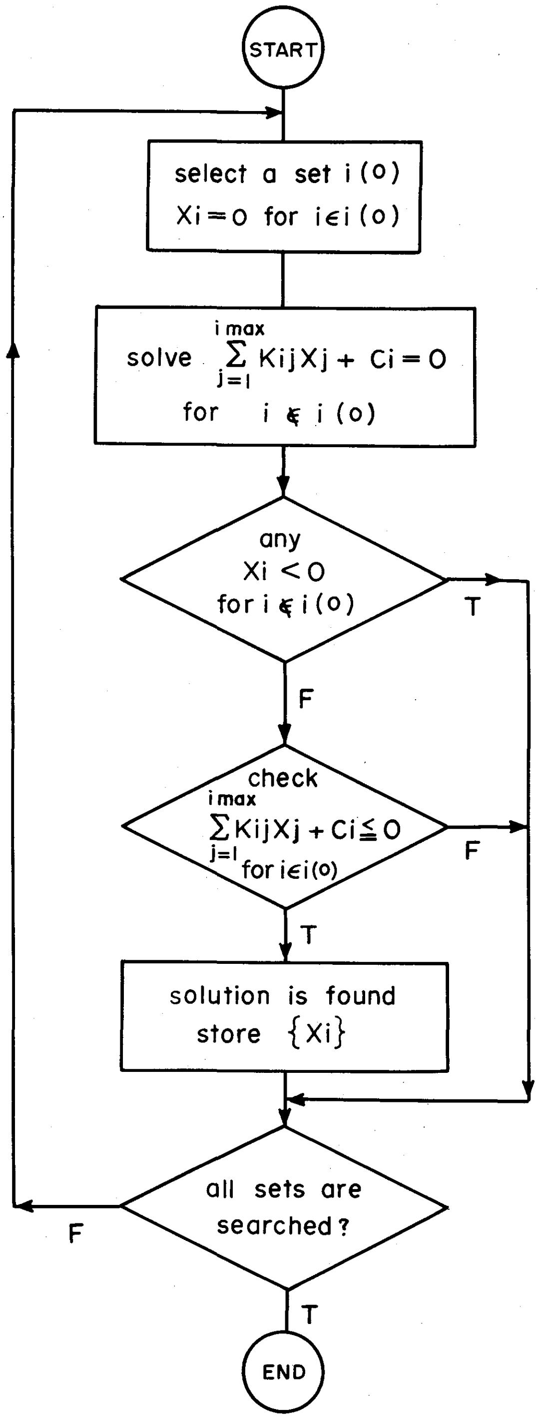

Fig. 7.9 Flow diagram for the exact direct method used in the MRI • GCM-I for solving the mass flux distribution equation.

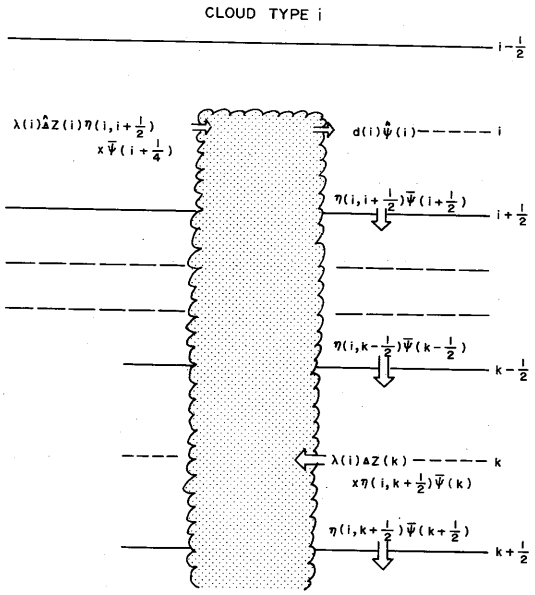

Fig. 7.10 A schematic diagram of the large-scale budget of ψ for type-i cloud.

$$\left\{\begin{array}{ll} x(i)=0 & \text{and} \\ \sum_{j=1}^{i\,max} K(i,j)\,x(j)+c(i)\leqq 0 & \end{array}\right. \tag{7.80b}$$

Schubert (1973) proposed an initial-value iterative method of solving the equation and Lord *et al.* (1982) discussed both a direct solution method and a linear programming method. It is mentioned that neither of these methods guarantee exact solutions. In the following we introduce, as an alternative, an "exact direct method" adopted in the MRI•GCM-I.

x(i) can be either positive or zero. Since there are two possibilities for each x(i), there are 2^{imax} possibilities in all. Suppose if i(0) be the set whose elements are non-existing cloud types. In other words, i(0) is the set which satisfies the condition below

$$x(i)=0 \qquad \text{for} \qquad i \in i(0) \tag{7.81}$$

The first step is to solve the equation (7.80a) for $i \notin i(0)$ by Gaussian elimination. The second step is to examine the solution, x(i) for $i \notin i(0)$. If $x(i)<0$ for any i, this set i(0) is not the right one, thus select another set and repeat the procedure from the beginning. Otherwise, we proceed the third step. The third step is to examine inequality conditions (7.80b) for $i \in i(0)$. If equations (7.80b) are satisfied, the solution is the right one and stored. This procedures are repeated 2^{imax} times. The exact direct method is illustrated in Fig. 7.9.

Although one set of solutions is uniquely obtained under usual circumstances, ther are unusual cases where two sets or more are obtained. In the A-S cumulus parameterization theory, no selection rule among sets of solutions is derived. Therefore, as the true set, we tentatively select the one which has the maximum number of existing cloud type. In case we have many sets of solutions of which numbers of existing cloud types are the same, we arbitrarily choose the first found set.

In the current MRI•GCM, the number of troposheric layers is 5. Then i_{max} is 5 at most and the number of possibilities that the exact direct method must examine is $2^5=32$ at most. Therefore, the exact direct method is not so time-consuming even if compared with other methods. And, of course, the exact direct method guarantees the exact solution except roundoff errors. In the 12-layer version, the search for possible penetrated cumuli with their top above $p=p_l=100$ mb is suppressed from the beginning currently.

7.8 The large-scale budget and cumulus cloud feedback on the large-scale fields.

Lower part of Fig. 7.10 shows the large-scale budget of ψ(h or q) for layer k and type -i cloud. The downward fluxes of $\bar{\psi}$ per unit cloud base mass flux at the top and the bottom of the layer are given by η (i, k$-$1/2) $\bar{\psi}$ (k$-$1/2) and η (i, k+1/2) $\bar{\psi}$ (k+1/2), respectively. The entrainment of $\bar{\psi}$ is λ (i)Δz (k) η (i, k+1/2) $\bar{\psi}$ (k). Let δ_i [$\bar{\psi}$ (k)] represent a change in $\bar{\psi}$ (k) per unit m_b (i) and let the mass per unit area at layer k be Δp (k)/g, where Δp (k)= p (k+1/2)$-$p (k$-$1/2). Then the change in the large-scale budget of $\bar{\psi}$ is written as

$$\frac{\Delta p(k)}{g}\delta_i\,[\bar{\psi}(k)]$$

$$=\eta(i,\ k-1/2)\bar{\psi}(k-1/2)-\eta(i,\ k+1/2)\bar{\psi}(k+1/2)-\lambda(i)\Delta z(k)\eta(i,\ k+1/2)\bar{\psi}(k)$$

$$=\eta(i,\ k-1/2)\ [\bar{\psi}(k-1/2)-\bar{\psi}(k)]+\eta(i,k+1/2)\ [\bar{\psi}(k)-\bar{\psi}(k+1/2)] \quad (7.82)$$

Upper part of Fig. 7.10 shows the large-scale budget of ψ in the cloud top layer for the i-th cloud type. At the cloud top the detrainment of ψ per unit m_b(i) is d(i) $\hat{\psi}$(i). The downward flux of $\bar{\psi}$ at the layer is η(i, i+1/2) $\bar{\psi}$(i+1/2) and the entrainment of $\bar{\psi}$ is assumed to be λ(i)$\Delta\hat{z}$(i) η(i, i+1/2) $\bar{\psi}$ (i+1/4). Therefore, the counterpart to (7.82) for the cloud top layer is

$$\frac{\Delta p(i)}{g}\delta_i\,[\bar{\psi}(i)]=d(i)\ \hat{\psi}(i)-\eta(i,\ i+1/2)\ \bar{\psi}(i+1/2)$$

$$-\lambda(i)\Delta\hat{z}(i)\ \eta(i,\ i+1/2)\ \bar{\psi}(i+1/4)$$

$$=\eta(i,\ i+1/2)\ \{[1+\lambda(i)\Delta\hat{z}(i)]\ \mathrm{x}$$

$$[\hat{\psi}(i)-\bar{\psi}(i+1/4)]+\bar{\psi}(i+1/4)-\bar{\psi}(i+1/2)\} \quad (7.83)$$

In this model all detrained liquid water is assumed to evaporate instantaneously at the detrainment level. Consequently, the changes in $\bar{T}(k)$ and $\bar{q}_v(k)$ are calculated from δ_i $[\bar{h}(k)]$ and δ_i $[\bar{q}(k)]$ as

$$\delta_i\ [\bar{q}_v(k)] = \delta_i\ [\bar{q}(k)] \tag{7.84a}$$

and

$$\delta_i\ [\bar{T}(k)] = \frac{1}{C_p}\ \{\delta_i\ [\bar{h}(k)] - L\delta_i\ [\bar{q}(k)]\} \tag{7.84b}$$

The large-scale budget described above and the cumulus induced subsidence at the PBL top are used to compute the kernel elements. After solving mass distribution equation, results of the large-scale budget calculation are used for obtaining the cumulus feedback on the large-scale fields, too.

The total temperature and moisture changes at each level over the time Δt_d due to cumulus convection are given by

$$\left[\frac{\partial\ T\ (k)}{\partial t}\right]_{cc} \Delta t_d = \sum_{j=1}^{i\ max} \delta_j\ [\bar{T}\ (k)]\ m_b(j)\Delta t_d \tag{7.85a}$$

and

$$\left[\frac{\partial q_v(k)}{\partial t}\right]_{cc} \Delta t_d = \sum_{j=1}^{i\ max} \delta_j\ [\bar{q}_v(k)]\ m_b(j)\Delta t_d \tag{7.85b}$$

where the form of δ_j is given by (7.82) and (7.83). The cumulus mass flux at the PBL top, M_B is given by

$$M_B\Delta t_d = \sum_{j=1}^{i\ max} m_b(j)\Delta t_d \tag{7.86}$$

The amount of precipitation $P\Delta t_d$ is given by

$$P\Delta t_d = \sum_{i=1}^{i\ max} \left\{ \sum_{k=i+1}^{KB} C_0\Delta z(k)\ q_\ell{}^t(i,\ k-1/2)\ m(i,\ k-1/2) + \hat{C}_0\Delta\hat{z}(i)\ q_\ell{}^t(i,\ i-1/2)\ m(i,\ i-1/2) \right\} \Delta t_d \tag{7.87}$$

where $C_0 = 2 \times 10^{-3}\ m^{-1}$ and $\hat{C}_0 = 4 \times 10^{-3}\ m^{-1}$ (see section 7.5.4 for details).

Momentum changes due to cumulus convection are also computed in a similar way by assuming that momentum is conserved within cloud ensemble. Details are described in Chapter 11.

The cloudiness of cumulus clouds in the model is neglected, unless cloud top is above 400 mb level or 233°K level. If the cloud top is above such level, we regard that anvil clouds spread out as cirrus from the cloud top. The cloudiness of such cloud is set to unity at the cloud-top layer though its blackness is regarded as 0.5 in the radiation calculation. For details, see Chapter 13.

7.9 Ice phase parameterization

So far, we have not mentioned ice phase parameterization to avoid complexity. In the current MRI•GCM-I, the effects of ice phase are incorporated in a simple manner described below.

When the environmental temperature T (z) is less than the critical temperature T_{cr} (currently $-20°C$ is assumed), we introduce y defined below instead of h.

$$y=h+L_i q_v=c_p T+gz+L_f q_v \tag{7.88}$$

where $L_f=L+L_i$ and L is the latent heat of vaporization per unit mass of water vapor, L_i is the latent heat of fusion, and L_f is the latent heat of sublimation.

In the ice phase layer where $T(z)\leqq -20°C$, y is approximately conserved, while in the liquid phase layer where $T(z)>-20°C$, h is approximasely conserved. We assume that phase change occurs adruptly at the level of T_{cr}. Because of the difference between saturation water vapor pressure on ice and water, excess water vapor sublimates in the layer above. At the same time, cloud liquid water freezes and releases the latent heat. The temperature change due to those process at T_{cr} is

$$\Delta T=(L_f\Delta q+L_i \ell)/c_p \tag{7.89}$$

where ℓ is liquid water content, Δq is difference between the saturated mixing ratio on ice and on water. In the discrete model, temperature at the integer level $\bar{T}$ (k) is compared with T_{cr}. If $\bar{T}$ (k) is less than T_{cr}, the layer k is assumed to be the ice phase layer and the phase change is assumed to happen at the bottom of the layer k (*i. e.*, k+1/2 level).

These additional heating in the cloud due to phase change generates vouyancy and makes cloud work function larger. This means that cloud top is raised when the ice phase is included in the cumulus parametrizasion. We assume that precipitation from ice phase layer is in ice phase (*i. e.*, snowfall), and snowfall melts at 0°C level to cool the environment.

Although inclusion of ice phase makes the cumulus parameterization program complicated, its effect seems to be minor and not so significant.

A7.1 Some results from simulation studies

In this Appendix, we describe the selected results related to cumulus parameterization. Materials are taken from the forthcoming paper by Tokioka, Kitoh, Yagai and Yamazaki

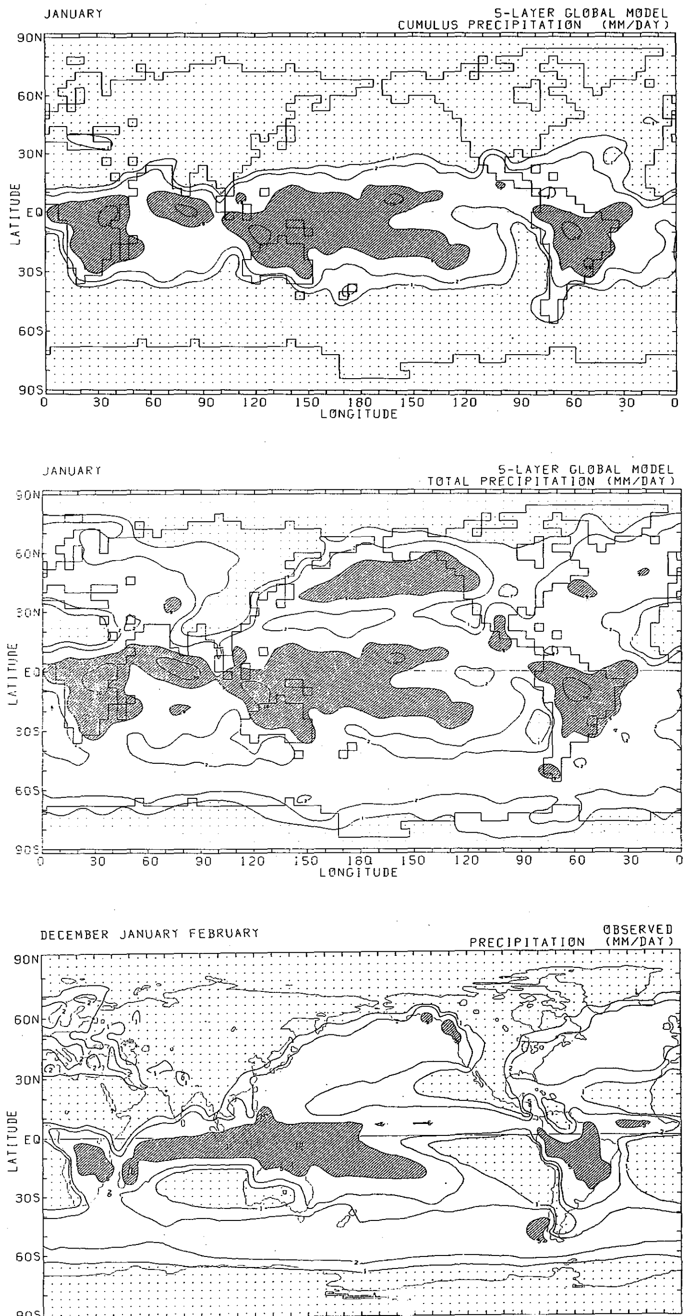

Fig. A7.1.1 January mean cumulus precipitation rate (top) and total precipitation rate (middle) simulated by the MRI • GCM-I. The observed precipitation rate for December, January and February is shown at the bottom. Contours are 1, 2, 5 and 10 mm day^{-1}. Regions greater than 5 mm day^{-1} are shaded and less than 1 mm day^{-1}, dotted. The observed data are from Schutz and Gates (1972).

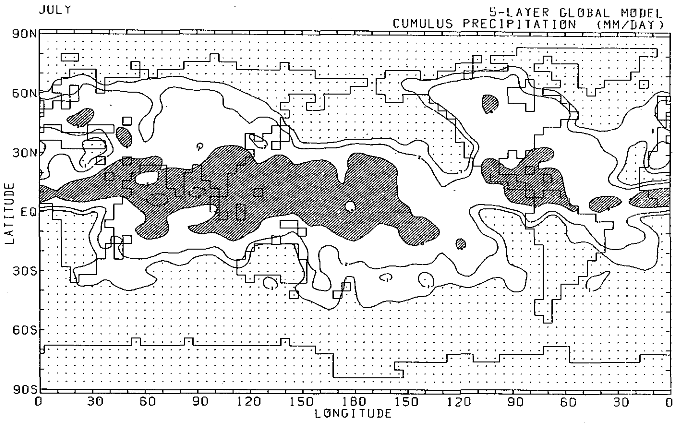

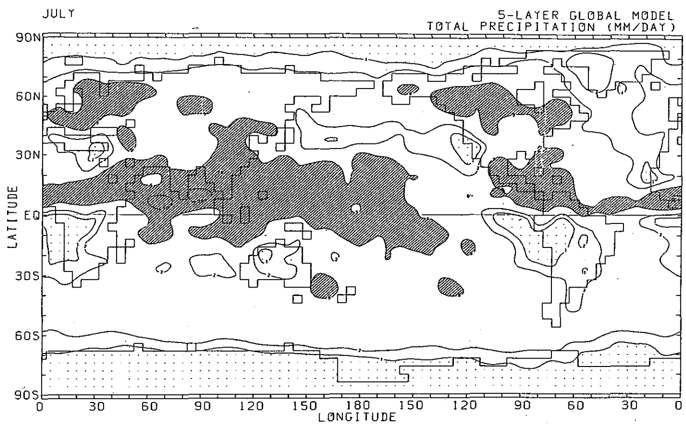

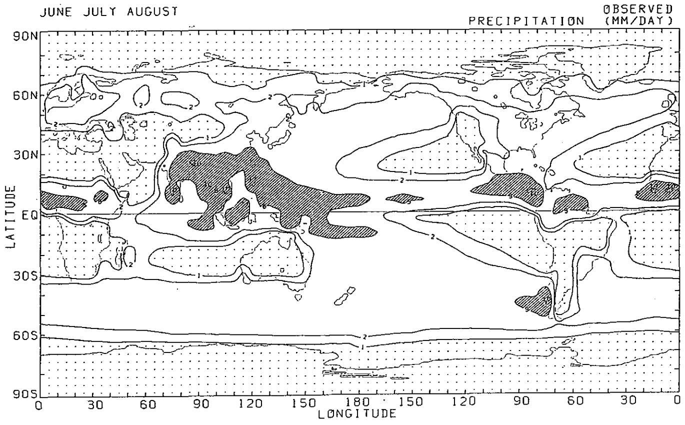

Fig. A7.1.2 Same as Fig. A7.1.1 except for July (top and middle) and June, July, August (bottom).

(1985) and Kitoh and Tokioka (1985). The simulation is made with the 5-layer tropospheric version of the MRI•GCM-I with a seasonal cycle.

A7.1.1 Precipitaion

Precipitaion in the model is produced through three processes, namely, large-scale precipitation, mid-level convection, and cumulus precipitation. Among them, precipitation caused by mid-level convection is small compared with other two. Figs. A7.1.1a and b show the cumulus and the total precipitation rates in the model for January. Cumulus precipitation is mainly produced in the tropical region (20°N-30°S). The cumulus precipitation accounts for most of the total precipitation there. It is also noted that the model favorably simulates the observed heavy precipitation area (see Fig. A7.1.1c), namely, north equatorial Pacific ITCZ, band-like area extending from the equatorial Pacific Ocean to the southeastern Pacific, the area over Indonesia extending to northern Australia, the ITCZ over equatorical Indian Ocean, the area from central Africa to Madagascar Island, and the area over Brazil. Although the central Atlantic ITCZ in the model is not active, precipitation is maximum there. The simulated amount of precipitation shows relatively good agreement with the observed amount, although the simulated one is slightly larger than the observed.

The distribution of precipitation rate for July is shown in Fig. A7.1.2. Over the tropical region, precipitation mainly consists of cumulus precipitaion. Noticeable observed features are well simulated by the model. The heavy precipitation area along 10°N latitude over the African continent, the north Atlantic ITCZ, the area extending from the northern part of Brazil to the central America, the ITCZ over north equatorial Pacific starting from southeast Asia, high precipitation band along 5-10°S over south central Pacific, and the monsoon area over India and Indian Ocean are among them. Though, there are a few deficiencies in the precipitation of the model. The ITCZ over north central Pacific is broad and extends to too far north in the model, which corresponds to insufficient southward expansion of subtropical high pressure over north Pacific. There also are fictitious heavy precipitation area over the western Arabian Sea and southern Arabian Peninsula.

Cumulus clouds produce heavy precipitation not only over tropical region, but also over mid-latitude continent in the summer hemisphere. The preicipitation over summer mid -latitude continent in the model is too high compared with the observation. This may allude some shortcomings of the model's ground hydrology and/or cumulus parameterization. Suarez and Arakawa (1981) showed that the ground wetness and cumulus convection have

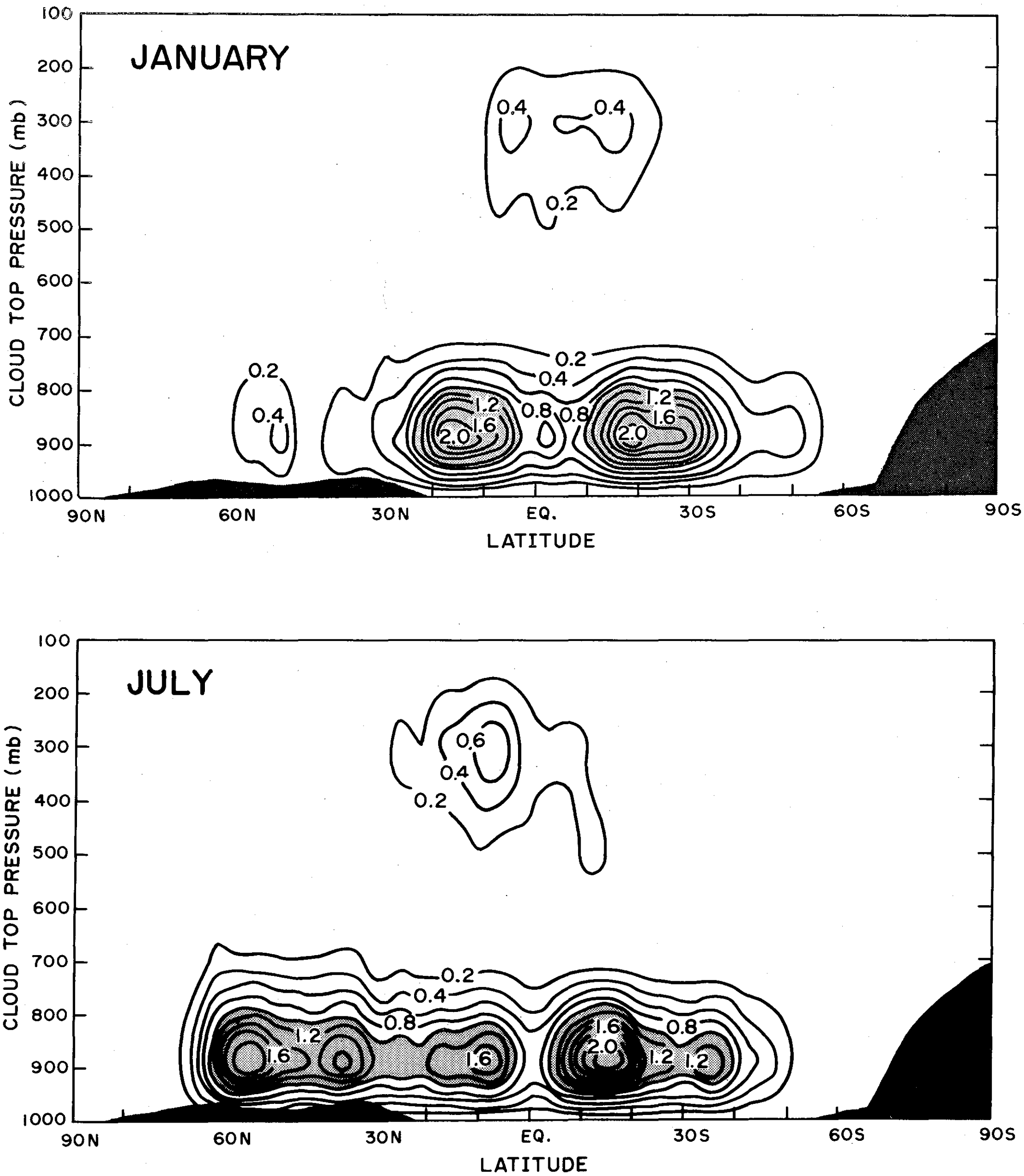

Fig. A7.1.3 Simulated zonal mean cloud base mass flux $m_b(P_d)$ for January (top) and July (bottom). Note that the ordinate indicates the cloud top pressure. Contour interval is 0.2 mb/hour. Values larger than 1 mb/hour are ahaded.

positive feedback due to enhanced tranfer of moisture through diurnal change of the PBL depth. Therefore, precipitation over summer continent is very sensitive to the ground wetness. Most of the cumulus precipitation over mid-latitude continent are caused by shallow clouds. Hence, the present cumulus parameterization may overestimate precipitation from shallow clouds.

A7.1.2 Cumulus cloud base mass flux.

Fig. A7.1.3 shows the zonal mean cloud base mass flux for January and July. Over tropics, bi-modal mass flux distribution is noticeable, namely the deep clouds, whose top lie at 300mb, and shallow clouds (~900mb) are predominant. In January the peaks of deep cloud mass fluxes are located at 5°N and 15°S, whereas in July, one peak appears at 10°N. The shallow cloud dominates over the subtropical region. In July, shallow cloud extends to mid-latitude (~60°N). As seen in subsection A7.1.1, this mid-latitude shallow cloud is predominant over the continent and produces excessive amount of precipitation there.

A7.1.3 Comparison with Marshall Islands data.

Yanai, Chu, Stark and Nitta (1976) analyzed the upper air and surface observation in the Marshall Islands region from 15 April through 22 July, 1956. They computed the mean apparent heat source and moisture sink by the budget analysis and estimated the cloud base mass flux m_b as a function of detrainment level by using the spectral cloud ensemble model similar to the model described in this chapter. Fig. A7.1.4 shows Yanai *et al.*'s estimate and results of the five-layer MRI•GCM-I over the corresponding region (average of values at 6 grid points within the square enclosed by 6°N, 10°N, 160°E, and 170°E) for the same season. The observation clearly shows the dominance of mass fluxes associated with very shallow and very deep clouds. The model's calculation shows the similar pattern, but the mass fluxes are much smaller than the observed ones (note the difference of the vertical resolutions between observation and simulation). The dominant deep cloud in the model has its top at 300 mb level, whereas the observed one has at 125 mb level. In the observation shallow clouds have much mass flux than deep clouds, whereas the simulation shows opposite feature. The observed precipitation rate is 10.1 mm/day and simulated one is 7.2 mm/day which is 30% less than the observed.

There might be ambiguity in the observation and large interannual variability of cumulus activity over the equatorial Pacific region. However, comparison of simulated results and

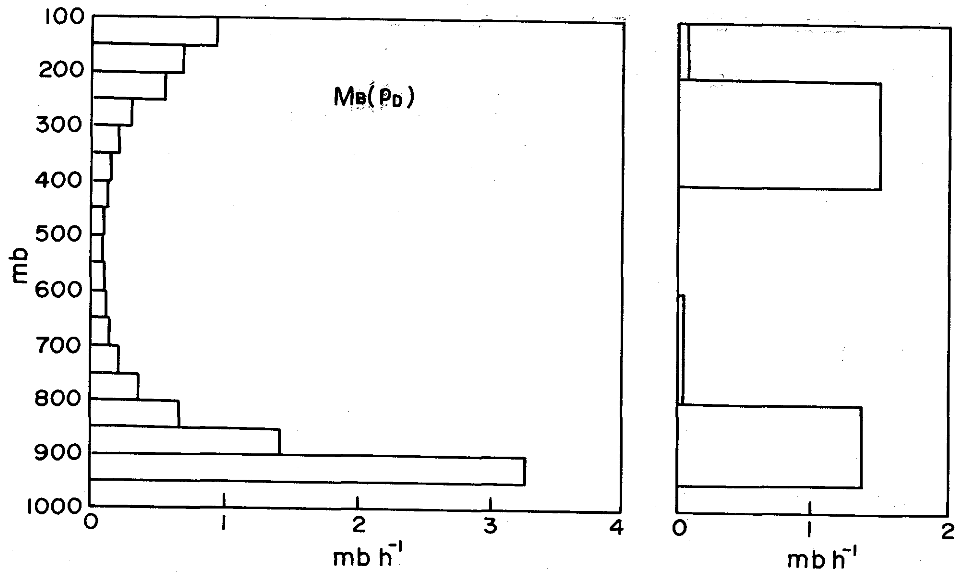

Fig. A7.1.4 The observed (left) and the simulated (right) mean cloud base mass flux $m_b(P_d)$ over the Marshall Islands region during the period 15 April through 22 July. The observed data are taken from Fig. 5 of Yanai *et al.* (1976). See text for details.

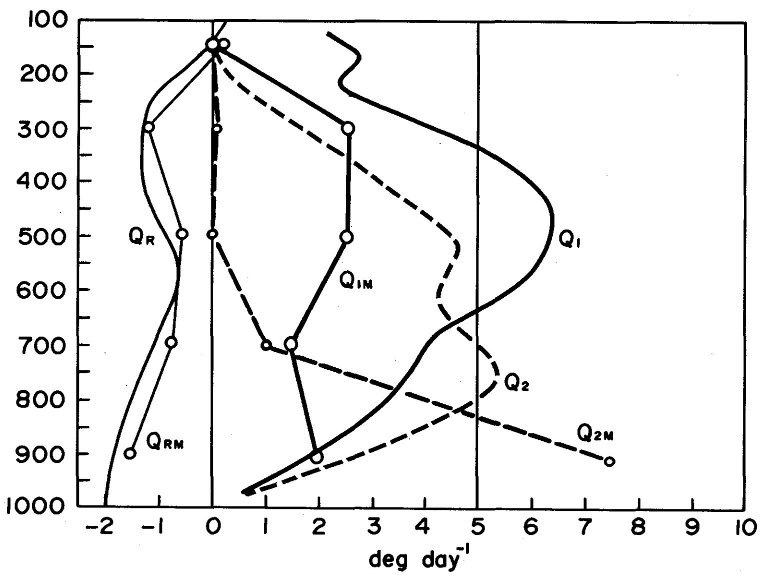

Fig. A7.1.5 The mean apparent heat source Q_1 (solid), moisture sink Q_2 (dashed) and radiational heating rate Q_R (thin solid) given by Dopplick (1970) over the Marshall Islands region. Adopted from Yanai *et al.* (1976). Simulated results by the MRI • GCM-I are also shown by corresponding lines with small open circles. The suffix M indicates the simulated values by the model.

observation seems to allude the drawback in the cumulus model. The drawback can be seen more clearly in the apparent heat source Q_1 and moisture sink Q_2 (Fig. A7.1.5). Q_1 in the model is the rate of temperature change due to cumulus clouds, Q_2 is the rate of change of $-L\ q_v$ due to cumulus clouds. Q_1 and Q_2 in the model are less than the observed values except in the lowest layer. For the lowest layer, cumulus clouds in the model make the environment too dry.

A7.1.4 Cloudiness

The simulated zonally averaged total cloudiness in July is shown in Fig. A7.1.6, together with the observed one (Dopplick, 1979). As mentioned in section 7.8, the cloudiness of cumulus cloud is zero except anvil of cirrus cloud. Fig. A7.1.6 shows that the model underestimates the cloudiness over tropics. The shallow cloud is responsible for this discrepancy between the simulation and observation. As far as radiation is concerned, shallow clouds act to cool the middle and upper troposphere. The Hadley circulation in the model is somewhat weaker than

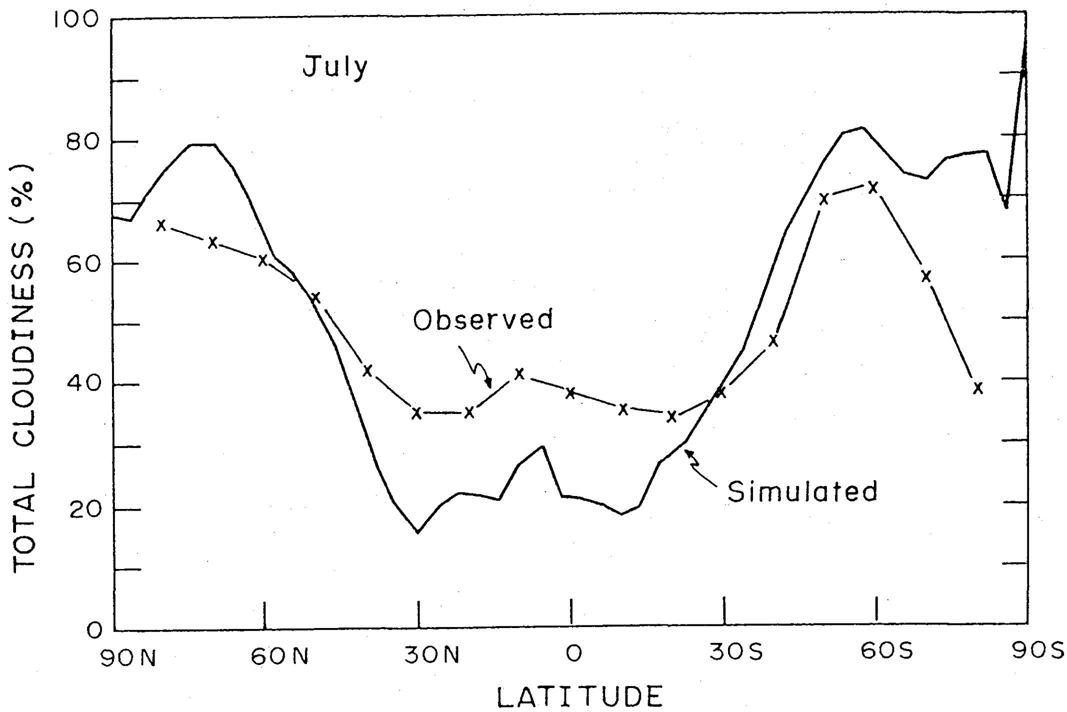

Fig. A7.1.6 The solid line shows the latidudial distribution of the zonally averaged total cloudiness (%) for July. The observed distribution is shown by thin solid line with crosses and taken from Dopplick (1979).

observation (Tokioka *et al*., 1985, Kitoh and Tokioka, 1985). Therefore, magnitude of the Hadley cell may become stronger by taking into account of shallow cloudiness into the radiation calculation.

The model simulates the precipitation pattern relatively well. But, there are some drawbacks in the simulated results such as too much precipitaion over summer extratropic continent, too much dryness of the low layer in the tropics. The origin of these drawbacks probablely does not lie soley in the cumulus parametrization. Nevertheles, it is necessary to seek for the improvement and sophistication of cumulus parameterization for better simulation by the GCM.

A7.2 Simple examples of the solution for the mass flux distribution equation

The simple 2nd order equation will be considered to elucidate the character of the mass flux distribution equation. Cloud type 1 is regarded as deep cloud ensemble and cloud type 2 as shallow cloud ensemble. Without loss of generality, we can assume the diagonal elements of K matrix are -1.

Example 1.

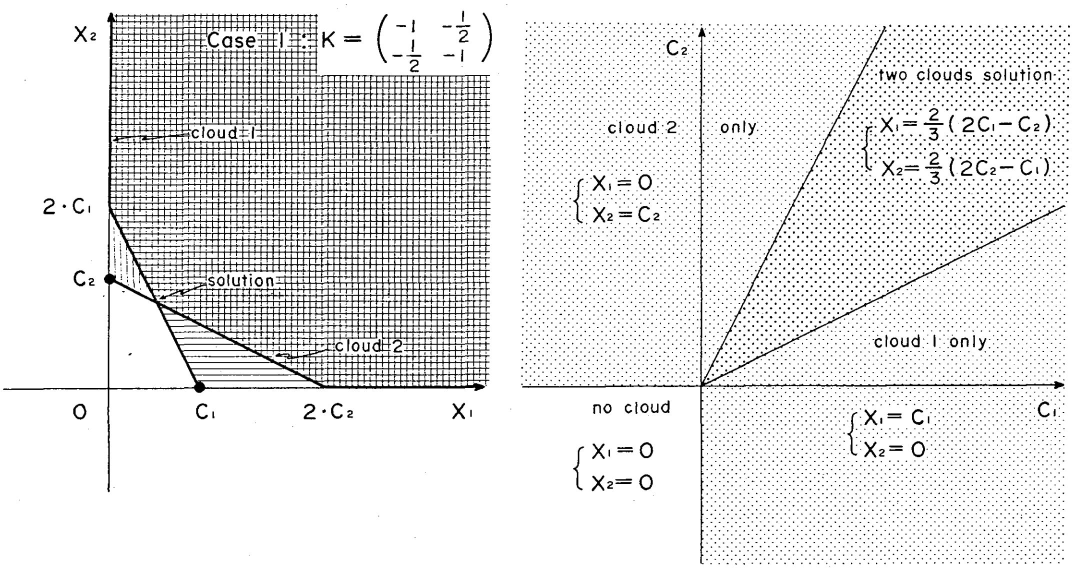

Fig. A7.2.1 Graphical representations of the equation (left) and solutions (right) for example 1. See text for details.

$$K=\begin{bmatrix} -1 & -1/2 \\ -1/2 & -1 \end{bmatrix}$$

The graphical representation of the equation for cloud 1 and 2 is shown in Fig. A7.2.1. A unique solution is found at the intersection point of two lines. The solution is shown on the two dimensional forcing C_1-C_2 plane in the right hand side of Fig. A7.2.1. When the forcings for both clouds are comparable, both clouds can exist. When the forcing for the certain cloud is negative, such cloud can not exist. In any case, the solution is unique. Fig. A7.2.2 shows the variation of mass flux x_1 with forcing C_1 when C_2 is fixed. It is seen that the cloud-cloud interaction has reduced the mass flux when the forcing C_1 is less than 2 C_2.

Example 2.

$$K=\begin{bmatrix} -1 & 1/2 \\ -1/2 & -1 \end{bmatrix}$$

In this case K (1, 2) is positive which means that the cloud 2 affects to enhance the cloud 1. The possibility that this type of situation occurs in the real atmosphere can not be excluded. In the special circumstances, the shallow cloud (cloud 2) might have an positive effect on the deep cloud (cloud 1) through the moistening process of the lower atmosphere at the top of the shallow cloud. Graphical representation of the equation and the solution are shown in Fig. A7.2.3 in the same manner as in Fig. A7.2.1. In this case even if the forcing for cloud 1 is negative mass flux of cloud 1 can have non-zero values. The solution for this example is also unique.

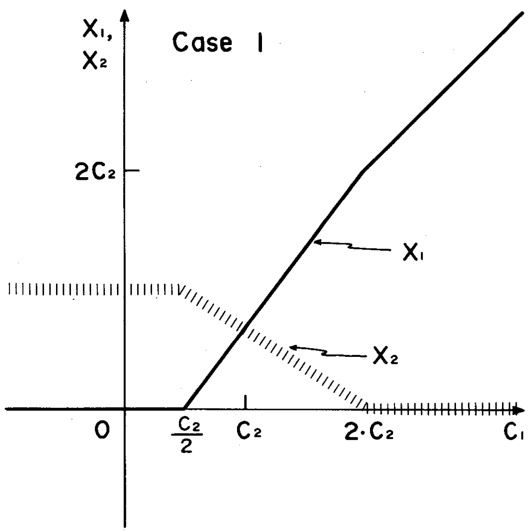

Fig. A7.2.2 Variations of the solutions with the cloud 1 forcing C_1 for example 1, provided the cloud 2 forcing C_2 is held constant. See text for details.

Example 3.

$$K=\begin{bmatrix} -1 & -2 \\ -2 & -1 \end{bmatrix}$$

In this case the interactions between two types of clouds are stronger than the self-interactions. Occurrence of such a situation is unlikely but possible in the GCM due to its coarse vertical resolution and/or any computational errors. There exist three solutions when

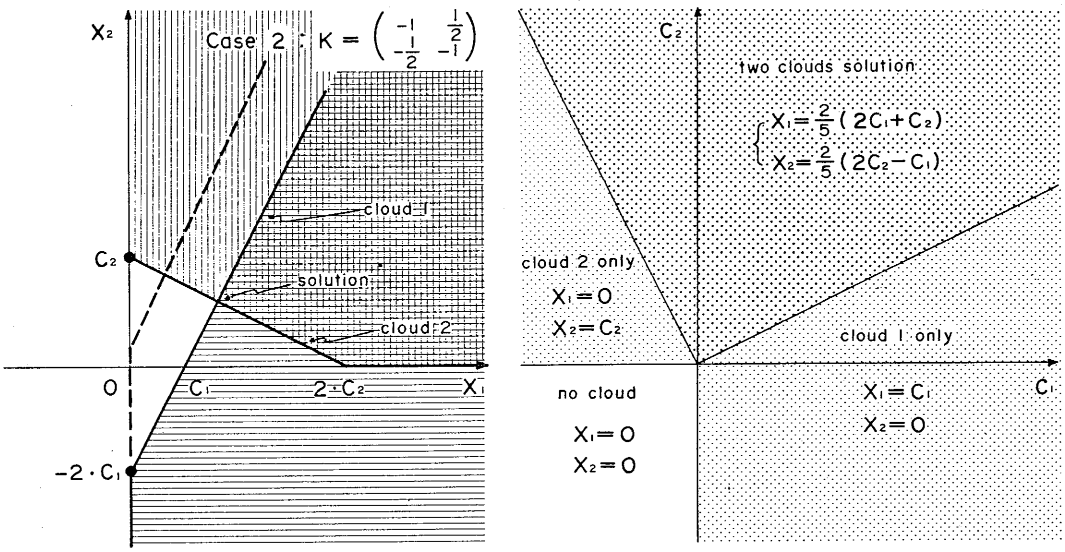

Fig. A7.2.3 Same as Fig. A7.2.1 except for example 2.

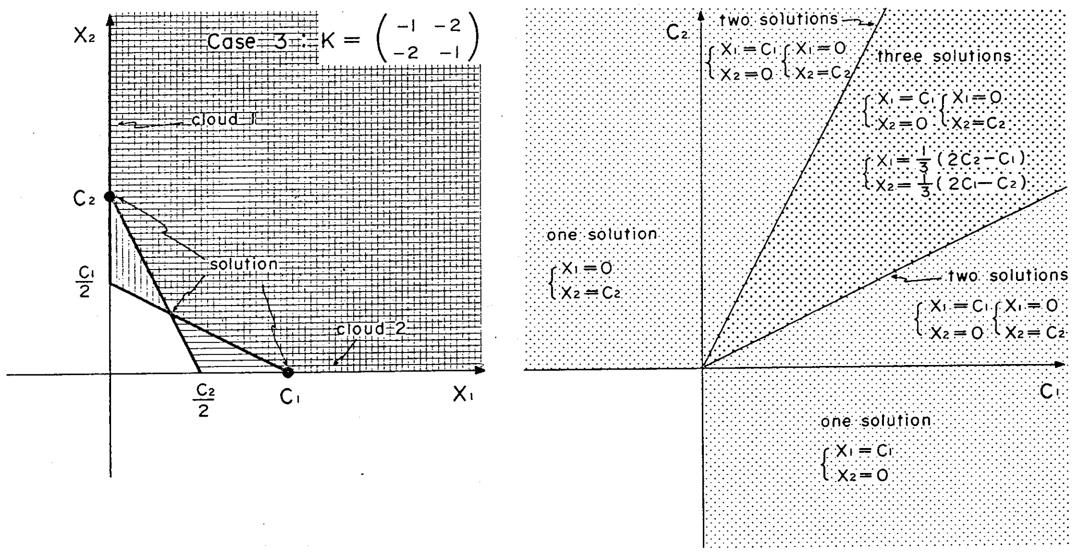

Fig. A7.2.4 Same as Fig. A7.2.1 except for example 3.

$C_2/2<C_1<2C_2$. (see Fig. A7.2.4). There is no selection rule among three solutions. Fig. A5 shows the variation of x_1 with C_1 when C_2 is fixed. Discontinuity of the solution takes place at $C_2/2$ and $2C_2$. Untill C_1 increases from zero to $C_2/2$, x_1 reamins zero. When C_1 is larger than $2C_2$, x_1 is C_1. Between $C_2/2$ and $2C_2$, x_1 can have three values. In this example, there is no unique solution.

It is of interest to check whether the right solution will be obtaind by the overadjustment simplex method proposed by Lord *et al.* (1982). In the overadjustment simplex method, the solution which minimizes linear objective function Z is searched, over the shaded region in Fig. A7.2.1, where Z is defined as

$$Z=\sum_{i=1}^{i\max} \left| \sum_{j=1}^{i\max} K(i, j)\, x_j+c_j \right| \tag{A7.2.1}$$

See Lord *et al.* (1982) for details. It is known that solution should occur at the extreme points on the boundary of the region. When x_1 and x_2 are positive, the solution given by the overadjust simplex method agrees with the right solution for examples 1 and 2. For example 3, however, the overadjustment simplex method can choose only one solution. Let us consider the simple case that $C_1=C_2=3$. In this case there are three solutions, namely, (x_1, x_2) equals to 1) (1,1), 2) (3,0), 3) (0,3). The simplex method chooses the first solution. Next let us consider the case that $C_1=3$, $C_2=1$. The right solution is (3,0). In this case, however, the overadjustment simplex method chooses (0,3/2) which is not the solution (see Fig. A7.2.5).

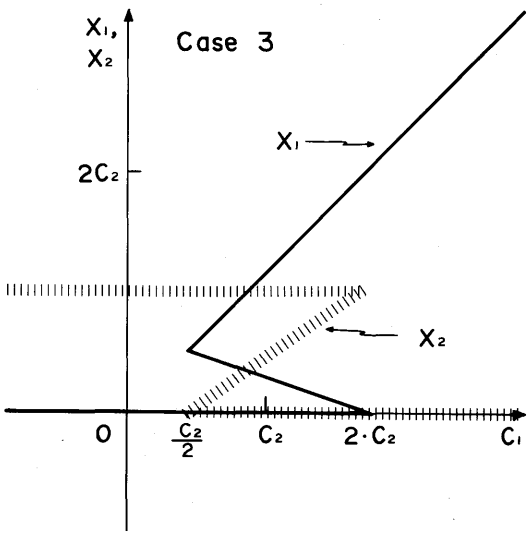

Fig. A7.2.5 Same as Fig. A7.2.2 except for example 3.

Theorem :

$$x_1+ax_2=C_1 \text{ and } x_1>0 \text{ or } x_1=0 \text{ and } ax_2\geqq C_1$$
$$bx_1+x_2=C_2 \text{ and } x_2>0 \text{ or } x_2=0 \text{ and } bx_1\geqq C_2 \tag{A7.2.2}$$

The necessary and sufficient condition for the above equation to have an unique solution is

$$1-ab\equiv D>0,\ \textit{i. e.},\ \det|-K|>0 \tag{A7.2.3}$$

There are four cases for the solution.

1) $x_1 = x_2 = 0$ then,

$$0 \geqq C_1 \tag{A7.2.4}$$

$$0 \geqq C_2 \tag{A7.2.5}$$

2) $x_1 = 0$, $x_2 > 0$ then,

$$a x_2 \geqq C_1 \tag{A7.2.6}$$

$$x_2 = C_2 > 0 \tag{A7.2.7}$$

3) $x_1 > 0$, $x_2 = 0$ then,

$$x_1 = C_1 > 0 \tag{A7.2.8}$$

$$b x_1 \geqq C_2 \tag{A7.2.9}$$

4) $x_1 > 0$, $x_2 > 0$ then,

$$x_1 = (C_1 - aC_2)/D > 0 \tag{A7.2.10}$$

$$x_2 = (C_2 - bC_1)/D > 0 \tag{A7.2.11}$$

We will show that these four cases are mutually exclusive provided $\det |-K| > 0$.

Proof :

Suppose case 1) holds ;

Then it is clear that case 2) and 3) contradict the case 1).

Suppose 4) holds too.

Then, from (A7.2.3) and (A7.2.10)

$C_1 - aC_2 > 0$ then $C_1 > aC_2$.

From (A7.2.4), $0 > aC_2$.

Then $a > 0$ from (A7.2.5)

From (A7.2.11) $C_2 - bC_1 > 0$

Multiply $a > 0$ to the above equation and after slight manipulation, we get

$C_1 - aC_2 < C_1\ (1 - ab) < 0$

This contradicts the condition (A7.2.10).

Suppose case 2) holds.

Suppose case 3) also holds, then $C_1 > 0$, $C_2 > 0$, $a > 0$, $b > 0$.

From (A7.2.6), (A7.2.7), (A7.2.8), and (A7.2.9)

$aC_2 \geqq C_1$

$bC_1 \geqq C_2$

Then $abC_2 \geqq bC_1 \geqq C_2$

$-(1 - ab)\ C_2 \geqq 0$ This lead to a contradiction to (A7.2.3).

Suppose case 4) also holds, then $aC_2 \geqq C_1$. We can derive the relation

$0 \geqq C_1 - aC_2$ which contradicts (A7.2.10).

We can easily lead the contradiction for case 3) as same as case 2).

Let us check the determinants for the previous examples.

Example 1 : $\det|-K| = 3/4$

Example 2 : $\det|-K| = 5/4$

Example 3 : $\det|-K| = -3$

Therefore, the examples 1 and 2 have their unique solutions while the example 3 does not.

For the equation of general order, the necessary and sufficient condition to have a unique solution is that all the small determinants $\det|-K'|$ are positive. But this theorem has not been proved yet.